

First partial skeleton of *Delphinornis larseni* Wiman, 1905, a slender-footed penguin from the Eocene of Antarctic Peninsula

Piotr Jadwiszczak and Thomas Mörs

ABSTRACT

The oldest fossil record of Antarctic penguins comes from Seymour Island (Antarctic Peninsula) and dates to the Paleocene and Eocene. The Paleocene bones are extremely rare, whereas specimens from the latter epoch are numerous. Despite the recent discoveries of incomplete skeletons assignable to the giant penguins from the Eocene of Antarctic Peninsula, the reliable systematics of their smaller contemporaneous relatives, known from isolated bones, have remained dependent on the tarsometatarsus. Here, new data on the skeleton of *Delphinornis larseni*, the most abundant among non-giant Eocene penguins, are reported. The specimen, collected from the Submeseta Formation on Seymour Island, comprises the incomplete pelvis and numerous bones from the hind-limb skeleton, including a well-preserved (diagnostic) tarsometatarsus. The acetabular foramen is, like in larger fossil penguins, clearly smaller than the elongated ilioischiatric foramen. The area of the latter opening, not occupied by the connective-tissue sheet, supposedly accounted for one-third of the foramen. We propose that the ischiadic artery was, unlike in present-day penguins, the main blood vessel supplying most of the hind limb. The proximal fovea of the femoral head is uniquely preserved, revealing an osteological aspect of the bone-ligament interface. We surmise that the individual was similar, in terms of body size, to extant *Pygoscelis papua*, but was characterized by more elongate feet. In our opinion, it was probably a young bird, up to several years old.

Piotr Jadwiszczak. Institute of Biology, University of Białystok, K. Ciołkowskiego 1J, 15-245 Białystok, Poland. piotrj@uwb.edu.pl

Thomas Mörs. Department of Paleobiology, Swedish Museum of Natural History, P.O. Box 50007, SE-104 05 Stockholm, Sweden. thomas.mors@nrm.se

Keywords: Antarctica; Seymour Island; Late Eocene; early Sphenisciformes; *Delphinornis larseni*; new material

Submission: 18 October 2018. Acceptance: 15 May 2019.

Jadwiszczak, Piotr and Mörs, Thomas. 2019. First partial skeleton of *Delphinornis larseni* Wiman, 1905, a slender-footed penguin from the Eocene of Antarctic Peninsula. *Palaeontologia Electronica* 22.2.32A 1-31. <https://doi.org/10.26879/933>
palaeo-electronica.org/content/2019/2574-skeleton-of-an-eocene-penguin

Copyright: June 2019 Paleontological Society.

This is an open access article distributed under the terms of Attribution-NonCommercial-ShareAlike 4.0 International (CC BY-NC-SA 4.0), which permits users to copy and redistribute the material in any medium or format, provided it is not used for commercial purposes and the original author and source are credited, with indications if any changes are made.
creativecommons.org/licenses/by-nc-sa/4.0/

INTRODUCTION

Present-day penguins (Aves, Sphenisciformes) are the most distinct among orders of birds. All of them are flightless, wing-propelled marine divers that can be found across the Southern Hemisphere (e.g., Williams, 1995). Such a characteristic held true also for their Paleogene (66–23 Ma) antecedents, which is unambiguously documented by their fossil record (Slack et al., 2006; Jadwiszczak, 2009; Ksepka and Ando, 2011; Mayr et al., 2018). These highly derived seabirds presumably originated in the Cretaceous (145–66 Ma) (e.g., Slack et al., 2006) or the Paleocene (66–56 Ma) (e.g., Jarvis et al., 2014). The earliest skeletons attributable to Sphenisciformes, found on New Zealand and Seymour Island (Antarctic Peninsula), are Paleocene in age (Tambussi et al., 2005; Slack et al., 2006; Jadwiszczak et al., 2013; Mayr et al., 2017a, 2017b, 2018). The fossil record of Eocene (56–34 Ma) penguins is by far more abundant. During this epoch, Sphenisciformes became widespread, expanding their ranges to Australia (e.g., Park and Fitzgerald, 2012) and lower latitudes, ultimately reaching the equatorial coastal region of western South America (Clarke et al., 2007). Nevertheless, in terms of the phylogenetic approach to classification, they were representatives of a stem group (e.g., Clarke et al., 2003).

Remains of Eocene Antarctic penguins are known solely from NE part of Seymour Island (Figure 1.1–2). They are more numerous and diverse than fossils representing contemporary assemblages of Sphenisciformes from other continents (Jadwiszczak, 2009). A growing body of evidence suggests that 10 species, widely accepted to be distinct (Myrcha et al., 2002; Jadwiszczak, 2009; Ksepka and Ando, 2011), do not fully reflect the actual and apparently larger taxonomic diversity (Jadwiszczak, 2008, 2013; Acosta Hospitaleche et al., 2017b; Jadwiszczak and Mörs, 2017). Because a vast majority of fossils had been merely isolated bones, differential taxonomic diagnoses were based on the most characteristic skeletal elements – tarsometatarsi (see Myrcha et al., 2002). Other specimens were compartmentalized by means of indirect reasoning, grounded mainly on size differences (e.g., Jadwiszczak, 2006).

Recent discoveries of partial skeletons including tarsometatarsi belonging to giant Sphenisciformes from Antarctica, *Palaeudyptes gunnari* (Wiman, 1905), and *P. klekowskii* Myrcha et al., 1990, have shed some light onto the body plan of these intriguing birds (Acosta Hospitaleche and

Reguero, 2010, 2014). Specimens assignable to extremely large-sized penguins from the Eocene of Seymour Island, especially from the genus *Palaeudyptes* Huxley, 1859, clearly outnumber those belonging to their smaller relatives (Myrcha et al., 2002; Jadwiszczak, 2006). On the other hand, the most abundant in named species is another genus, *Delphinornis* Wiman, 1905, a representative of the latter group. Estimated body sizes of individuals from all its species (Jadwiszczak, 2011; Jadwiszczak and Mörs, 2011), i.e., *D. larseni* Wiman, 1905, *D. gracilis* (Wiman, 1905), and *D. arctowski* Myrcha et al., 2002, were largely comparable to those of middle-sized extant penguins (Jadwiszczak and Chapman, 2011, figure 1).

Up until now, very little research has been published on the partial skeleton of these relatively small Eocene Antarctic penguins, a noteworthy exception being a brief note on an incomplete wing tentatively assigned to *Delphinornis* (Jadwiszczak, 2010). The only specimens unequivocally assignable to this taxon have been tarsometatarsi (e.g., Myrcha et al., 2002). Here, we report on the only known set of skeletal elements of an individual unambiguously attributable to *D. larseni*, the most common non-giant Eocene penguin and type species of its genus, vastly expanding the knowledge of modest-sized representatives of early Sphenisciformes.

MATERIALS AND METHODS

The skeletal material described here was collected by TM in February 2012 on a plateau below and south-east of the Argentinian Marambio Base, close to a small depression that is often filled with melting water during the austral summer (“Site at the Lake”; Figure 1.2, 1.4). Here, a fossiliferous horizon is exposed that is very rich in penguin bones. The “Site at the Lake” is part of the Argentine locality DPV 13/84 (64°14'47"S, 56°36'12"W) and of locality no. 11 of the Swedish South Polar Expedition (Andersson, 1906; Acosta Hospitaleche et al., 2017a) (Figure 1.2, 1.4). Apart from penguin bones, this locality has produced remains of teleost fishes, a single *Carcharocles* shark tooth, a rostrum of a “pseudotooth” bird (Pelagornithidae), and whale bones (Wiman, 1905; Bargo and Reguero, 1998; Kriwet et al., 2016). The plateau exposes the middle part of the Submeseta Formation (Submeseta II = level 38) according to Montes et al. (2013), or Telm 7 of the La Meseta Formation according to Sadler (1988) (Figure 1.2–4). Most authors regard this part of the depositional succession on Seymour Island to be late Eocene (Pria-

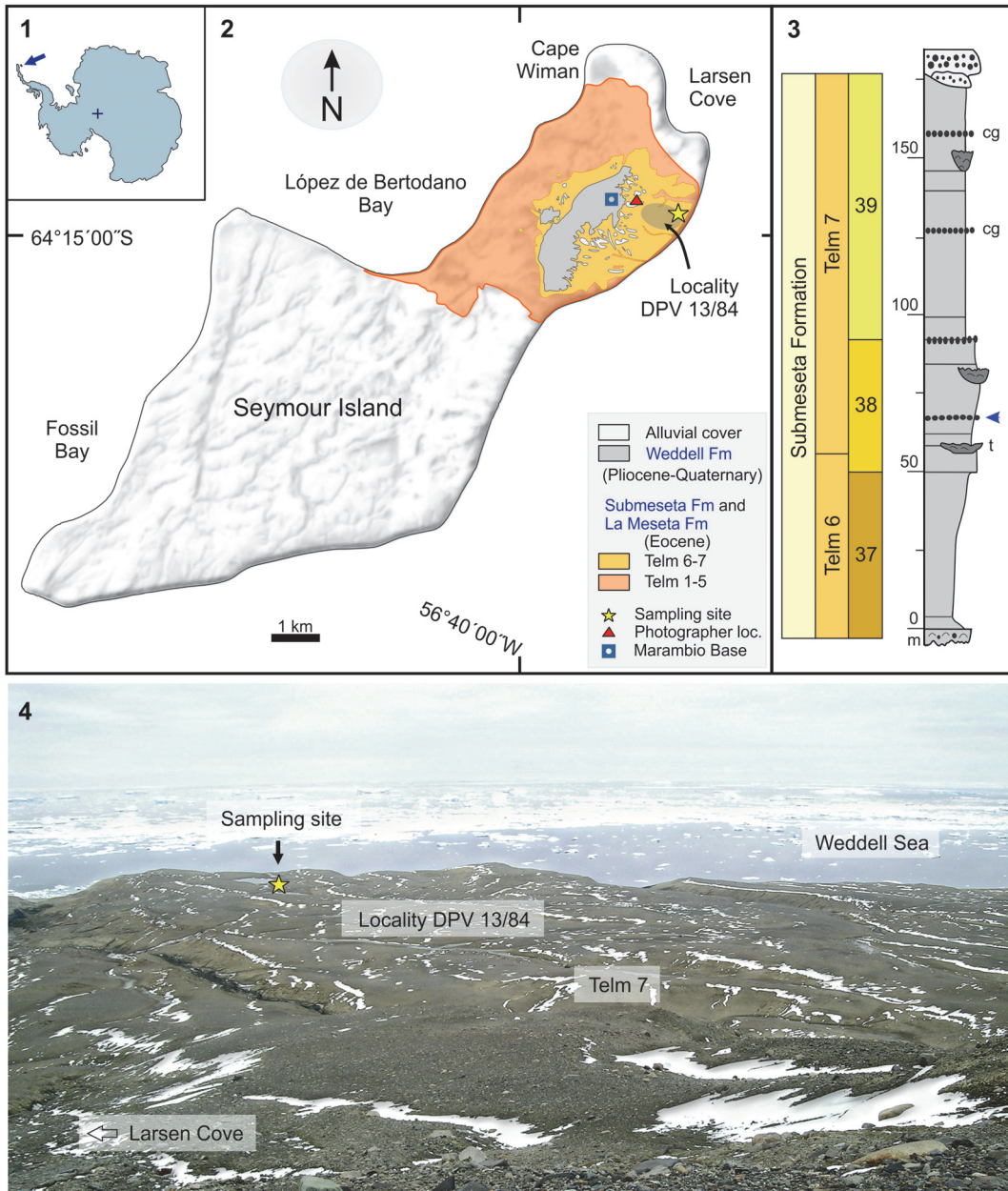


FIGURE 1. Location of Seymour Island (Antarctica) and stratigraphy of its NE part. 1. Map of Antarctica showing the position of Seymour Island. 2. Map of Seymour Island showing the location of the Eocene La Meseta and Submeseta formations, and position of the locality DPV 13/84 with sampling site. 3. Simplified stratigraphic column of the Submeseta Formation with an arrow pointing at the sampling horizon, based on data from Montes et al. (2013). 4. View of the sampling site location from under the plateau of the Weddell Formation; photograph was taken in 2011 by TM. Abbreviations: cg, conglomerates and sandstones; t, *Turritella* (a gastropod).

bonian) in age (e.g., Marenssi, 2006; Douglas et al., 2014; Buono et al., 2016).

The fossil material is housed in the paleozoological collections of the Swedish Museum of Natural History, Stockholm. It was partially (manually) purged of matrix remnants in 2017. The comparative material studied directly comes from the

above-mentioned institution (fossils), the University of Białystok, Poland (fossils and a small number of recent bones), the Natural History Museum at Tring, UK (a vast collection of recent bones), and the Natural History Museum, London, UK (fossils). TM and PJ have been curators of Swedish and Polish collections (respectively); bones from Lon-

don and Tring were studied by PJ in 2011 and 2015, as part of the SYNTHESYS grants GB-TAF-987 and GB-TAF-4610 (respectively).

Photographs of penguin bones were taken using a digital single-lens reflex camera (20.9 megapixel image sensor, devoid of a low-pass filter) paired with 40 mm macro lens. Raw X-ray images of the new fossil material assignable to *D. larseni* were captured at 58 kV (kilovolts), 3.2 mAs (milliampere-seconds), distance from the (anode) focus of 100 cm, without anti-scattering grid, and digitally pre-processed following the protocol for canine limb joints (CRystalView software; Alara Team, 2005-2013). This “mammalian” protocol turned out to be the most suitable in the case of studied penguin remains. The heat map of the acetabular socket was created from an X-ray by means of Fiji (a redistribution of ImageJ program; Schindelin et al., 2012), using the 3D Surface Plot module (Thermal LUT mode). The heat map for a portion of the left tarsometatarsus was generated from an X-ray, using Sante DICOM Viewer Free program in NIH palette mode (Santesoft Team, 2018).

Shape analyses of outlines of major hip bone foramina were conducted using the Momocs package (version 1.2.9; Bonhomme et al., 2014) for R environment (version 3.4.3; R Core Team, 2017). This is a relatively easy-to-use, well-designed toolkit, with implemented methods for analysing the landmark-poor configurations. Shapes of acetabular and ilioischadic foramina belonging to representatives of eight present-day penguins (specimens from Bialystok and Tring) (Appendix 1), supplemented by those from the studied Eocene specimen, were extracted (black silhouettes, white background) from photographs taken by a single person (PJ; to control the viewing angle) and saved as jpg files (an acetabular-ilioischadic pair per file) (Appendix 2.1). To ensure each configuration is treated by a program as a single shape, a thin black line connecting extreme points of foramina was drawn prior to file creation. In the case of NRM-PZ A.994, because of imperfect specimen preservation, such a pair was based on combined images from left and right hip bones. Configurations for Paleocene and Oligocene penguins, used solely in a cladogram, were assessed based on published images (Slack et al., 2006, figure 1.A; Ksepka et al., 2012, figure 6.E-F).

The set of files was imported into the R/Momocs environment, converted into an Out-class object (a list of closed outlines) by means of Out function and inspected for errors using panel func-

tion (Appendix 2.2-3). To visualize the location of the Eocene specimen relative to the sampled extant-penguin morphospace, the contents of above object was aligned, centered, and scaled using package-supplied helper procedures, and plotted by means of stack function (Appendix 2.3).

Outline data were also used to compute elliptic Fourier transform (EFT) by means of efourier function, using 16 harmonics and other parameters set to their defaults. The number of harmonics (their sum approximates the outline) was based on a harmonic power analysis and visual inspection of reconstructed forms. The procedure resulted in normalized elliptic Fourier coefficients (outline-form descriptors; four per harmonic; Appendix 3) in a form of an OutCoe-class object. This normalized dataset was utilized, via PCA function, in Principal Component Analysis (PCA). It was also used, after reverse transformation from coefficients to shapes using mshapes to calculate and plot deformation grids between two (polarized) configurations. The latter step was performed by means of tps_grid function, and the choice of configurations was based on visual inspection of outlines and results of PCA (Appendix 4). For more details, see Appendix 2.3 as well as consult Bonhomme et al. (2014) and Momocs documentation.

The bubble chart for tarsometatarsal measurements was created using functionality of the ggplot2 package for R (Wickham, 2009). Measurements of comparative material (Appendix 1) were obtained both directly from specimens belonging to European collections (Bialystok, Stockholm and Tring) and from literature (Myrcha et al., 2002, table 1).

The anatomical nomenclature, in a form of English equivalents to Latin terms, follows Baumel and Witmer (1993) and Baumel and Raikow (1993). In some cases, in order to reflect peculiarities of penguin osteology, the terminology had to be adjusted. Body-size categories follow Williams (1995), and Jadwiszczak and Chapman (2011). Linear measurements were taken by means of a digital caliper and rounded to the nearest 0.1 mm.

Institutional Abbreviations

CM, Canterbury Museum, New Zealand; IB/P/B, University of Bialystok, Bialystok, Poland; MUSM, Natural History Museum of the National University of San Marcos, Lima, Peru; NHMUK, Natural History Museum, London, UK; NHMUK/T, Natural History Museum at Tring, UK; NRM-PZ, Museum of Natural History, Stockholm, Sweden; OU, Geology Museum, University of Otago, New Zealand.

SYSTEMATIC PALEONTOLOGY

Class AVES Linnaeus, 1758

Order SPHENISCIFORMES Sharpe, 1891 (also sensu Clarke et al., 2003)

Family SPHENISCIDAE Bonaparte, 1831 (but not sensu Clarke et al., 2003)

Genus DELPHINORNIS Wiman, 1905

Delphinornis larseni Wiman, 1905

Figures 2.1-7, 2.15, 2.17-19, 3, 4.2-6, 4.8-17, 5.3-4, 5.6, 5.8-9, 5.13, 5.16, 6

Material. Incomplete pelvis and leg skeleton including femur, tibiotarsus, fibula, tarsometatarsus and phalanges (NRM-PZ A.994); both body sides represented, partly in matrix.

Taxonomic Remarks

Suprageneric position of NRM-PZ A.994. The hierarchical system of classification places all penguin species, both extinct and extant, in a single family, Spheniscidae, within a monotypic order - Sphenisciformes (Simpson, 1946, 1971; Myrcha et al., 2002; Jadwiszczak, 2006, 2009). Therefore, within this framework, *D. larseni* is a member of Spheniscidae. Clarke et al. (2003) introduced a new context to the penguin systematics, treating these terms as the names of clades. The term Spheniscidae was suggested for the crown group, and this approach can be found in many later papers (e.g., Clarke et al., 2007; Ksepka and Ando, 2011; Ksepka et al., 2012). All extant genera of Sphenisciformes as well as other crown penguins are Miocene in age or younger (e.g., Ksepka and Ando, 2011; Gavryushkina et al., 2017), whereas all fossils assignable to pre-Miocene genera (including Eocene *Delphinornis*) and a number of younger findings represent the stem group (e.g., Ksepka and Clarke, 2010). In our work, we do not consider the cladistic/phylogenetic view as opposed to the traditional rank-based classification, but rather as another (informative) layer.

Generic and specific classification of NRM-PZ A.994. The complete tarsometatarsus discussed here (Figure 2.1-7, 2.18) is a small specimen, within the size range of non-giant penguins (Figure 3). Its hypotarsus, unlike in similarly-sized Eocene *Marambiornis* Myrcha et al., 2002 and *Mesetaornis* Myrcha et al., 2002 from Antarctica, is devoid of a groove separating the intermediate hypotarsal crests, and the medial crest slopes towards the medial margin of the bone (Figure 2.5-6). Considering the position of the medial vascular foramen (plantar view) and medial hypotarsal crest relative to the tarsometatarsal longitudinal axis, the former is abaxial (unlike in said genera) (Figure 2.5). This

set of traits is in line with the revised diagnosis for the genus *Delphinornis* enunciated by Myrcha et al. (2002).

The following combination of character states found in the bone in question is, according to Myrcha et al. (2002), diagnostic of *Delphinornis larseni*. The specimen is more elongated (elongation index of 2.76; a measure defined in Myrcha et al., 2002) than its counterparts in *Delphinornis arctowskii* (respective values do not exceed 2.5). It is also longer, in terms of absolute dimensions, than tarsometatarsi assignable to *D. arctowskii* and *Delphinornis gracilis* (Figure 3). The medial hypotarsal crest slopes quite gently (unlike in both congeneric species), gradually decreasing its steepness towards the medial margin of the bone. This is accentuated by the abrupt, albeit short, vertical drop to the edge of the second metatarsal (Figure 2.6). All three trochleae are relatively stout (Figure 2.2., 2.7), and the intercotylar eminence is quite wide and rounded (moderately pronounced) in dorsal view (Figure 2.1-2, 2.6) (unlike in *D. gracilis*). The preservation of both tarsometatarsi described above precludes decided assessments regarding the distal vascular foramen, which is well developed in the type specimen (e.g., Wiman, 1905, figure II.2) and some other specimens assignable to this species (e.g., Figure 2.9; see also revised diagnosis in Myrcha et al., 2002). We can state, however, that it is present in NRM-PZ A.994.

Comparative Description

Synsacrum. The sacral part of the pelvis is represented by two small fragments of the side wall of the canal of ankylosed vertebrae with conspicuous intervertebral foramina (Figure 4.3-6). Two best preserved foramina are indivisible, no separate openings for the dorsal and ventral roots of the spinal nerves are present. Such a condition can be observed in caudal, sacral and lumbar vertebral series of other synsacra assignable to Eocene Antarctic penguins (Figure 4.7; Jadwiszczak, 2006, figure 18.E, 2014, figure 1.C) and Oligocene *Kairuku waitaki* Ksepka et al., 2012 from New Zealand (Ksepka et al., 2012, figure 6.B). In lumbar part and lumbosacral transition, both types of openings can exist, and left and right side of the synsacrum may differ in this respect, even at the same level along the bone longitudinal axis (e.g., in IB/P/B-0149; Figure 4.7).

One of those foramina, belonging in a fragment connected through a piece of matrix with a cranial portion of the wing (ala) of the left ischium, is clearly larger and more rounded (Figure 4.5-6).

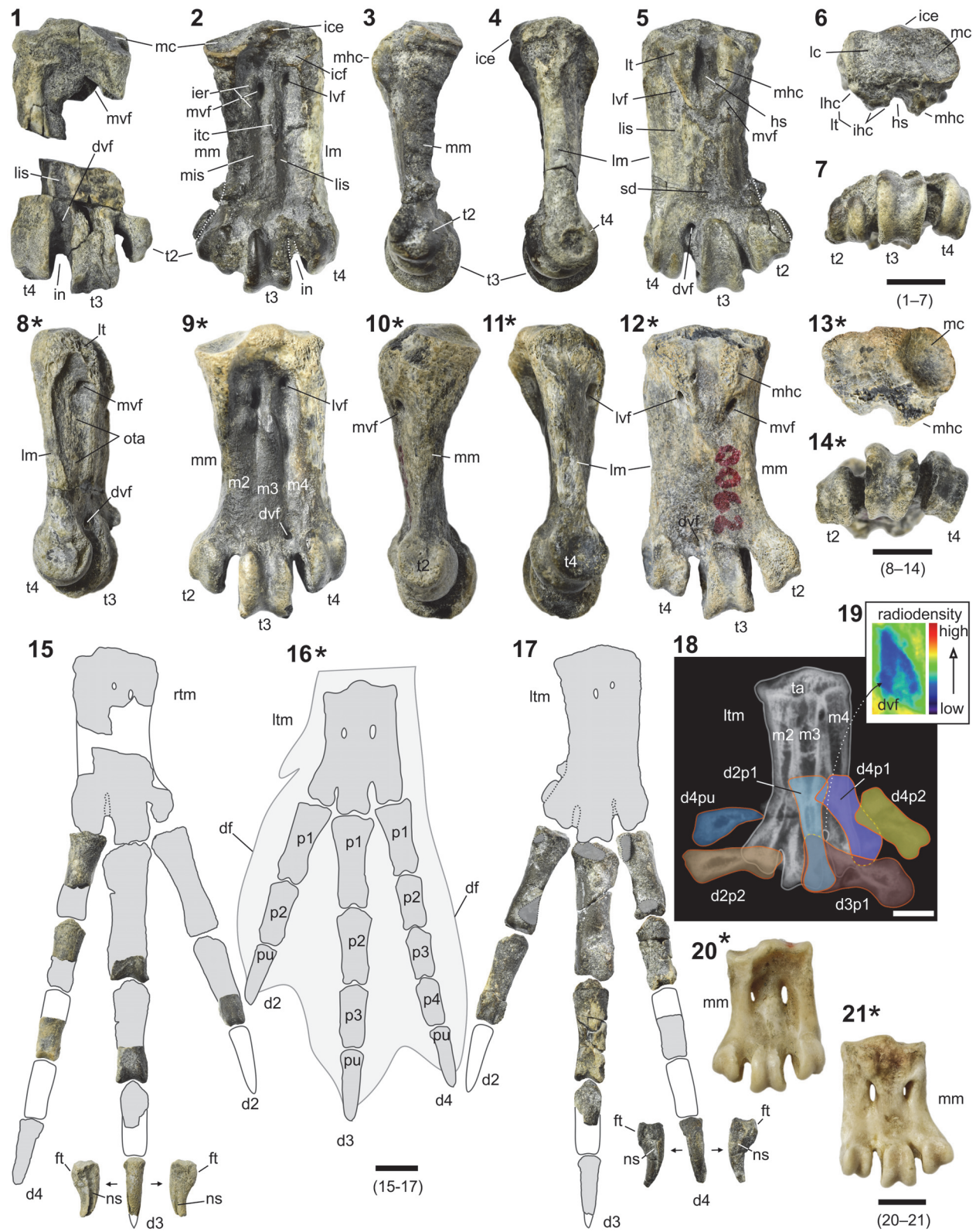


FIGURE 2 caption next page.

The other opening represents an element that diagenetically altered sediment associated with the body (corpus) of the left ischium and cranialmost pubis (accompanied by unrecognizable elements). It is elongated dorsoventrally and located between two protrusions of a supposedly inner surface of the wall (Figure 4.3-4).

Hip bones. The aforementioned two non-adjoining hip bone fragments contribute to partially preserved rims of three major openings: the acetabular, ilioischiadidic, and obturator foramina (Figure 5.7). The first structure is best preserved, showing approximately two-thirds of a roughly circular margin bounded by all three coxal/hip bones (Figure 4.2-3). Its diameter, estimated along the main bone axis in medial view, is ca. 13.6 mm, i.e., 118% of the value obtained by us for an unnumbered specimen (IB/P/B) of extant *Pygoscelis papua* (Forster, 1781) (Figure 5.12), 64% of the value reported for the largest living penguin, *Aptenodytes forsteri* Gray, 1844, and the Eocene individual from Tierra del Fuego, Argentina (Clarke et al., 2003, table 1), but merely 48% of that measured (by us) for the unassigned specimen (IB/P/B-0488; Figure 5.10-11) from the Eocene of Antarctica. The missing section corresponds to the preacetabular ilium, although a fragmentary iliac zone of the acetabular socket is retained. The acetabular foramen is “more or less regularly rounded in outline” in all birds (Kuznetsov and Sennikov, 2000, p. 441), including modern penguins (Zusi, 1975, figure 4.1; Stephan, 1979, figure 42). This is also evidenced for early Sphenisciformes from the Paleocene (Slack et al., 2006, figure 1A), Eocene (Clarke et al., 2003, figure 4.B; Jadwiszczak, 2006, figure

19.G; Acosta Hospitaleche and Olivero, 2016, figure 4.A) and Oligocene (Ksepka et al., 2012, figure 6.D-F).

The right hip bone is represented by a large part of the ilium (both pre- and post-acetabular wings), the body and incomplete wing of the ischium, and the cranial pubis, possibly also its caudalmost fragment (pubic apex) (Figure 5.2-4, 5.6). The acetabular foramen is devoid of a portion of its iliac margin, but overall the acetabulum is more complete than its left counterpart. The post-mortem deformation of its cranoventral part is apparent, especially in medial view (Figure 5.4). The medial opening is ca. 12.6 mm wide along the main bone axis, the lateral one is by ca. 2.5 mm wider. The inner surface of the socket seems to be very thin dorsally, as suggested by clear tapering of remaining fragments, sharp even at the level of the antitrochanter; Figure 5.4, 5.6, 5.8). It is not that thin in much larger IB/P/B-0488 (Figure 5.10-11) as well as other unfigured robust Eocene hip bones (IB/P/B-0625, IB/P/B-0627; see also Acosta Hospitaleche and Olivero, 2016, figure 4.A), whereas relevant smaller fossil specimens (e.g., IB/P/B-0211; Figure 5.5) are too incomplete to compare. The considered surface is also (relatively) wide in similarly-sized modern pygoscelid penguins (unnumbered specimens from IB/P/B; Figure 5.12). The antitrochanter (Figure 5.6) is well preserved, located expectedly caudodorsal to the lateral opening of the acetabulum, tongue-shaped (common for penguins), observed even in Paleocene *Waimanu manneringi* Jones et al., 2006 (in Slack et al., 2006; see Slack et al., 2006, figure 1.A) and moderately inflected laterally. The inflection varies in modern

FIGURE 2 (continued from previous page). Partial foot skeleton of Eocene *Delphinornis larseni*, NRM-PZ A.994. 1. Right tarsometatarsus in dorsal view. 2. Left tarsometatarsus in dorsal view. 3. Same in medial view. 4. Same in lateral view. 5. Same in plantar view. 6. Same in proximal view. 7. Same in distal view. 8. Left tarsometatarsus of *D. larseni*, IB/P/B-0547 (Eocene, Seymour Island, Antarctica), in lateroplantar view. 9. Left tarsometatarsus of *D. larseni*, IB/P/B-0062 (Eocene, Seymour Island, Antarctica), in dorsal view. 10. Same in medial view. 11. Same in lateral view. 12. Same in plantar view. 13. Same in proximal view. 14. Same in distal view. 15. Reconstruction of right-foot skeleton of *D. larseni* (NRM-PZ A.994) in dorsal view. 16. Outline of left-foot skeleton of extant *Pygoscelis papua* (unnumbered specimen from IB/P/B) in same view. 17. Reconstruction of left-foot skeleton of *D. larseni* (NRM-PZ A.994) in same view. 18. Schematic view of left-foot skeleton of *D. larseni* (NRM-PZ A.994) in dorsal view, as preserved in matrix, superimposed over X-ray image of same specimen. 19. X-ray-based heat map of portion of above fossil indicating location of tarsometatarsal d vf. 20. Left tarsometatarsus of *Pygoscelis papua* (unnumbered specimen from IB/P/B) in dorsal view. 21. Same in plantar view. Abbreviations: d2-4, digit 2-4; df, dermal flange; d vf, distal vascular foramen; ft, flexor tubercle; hs, hypotarsal sulcus; ice, intercotylar eminence; icf, infracotylar fossa; ier, impressions of extensor retinaculum; ihc, intermediate hypotarsal crests; in, intertrochlear notch; itc, insertion of tibial cranial muscle; lc, lateral cotyle; lhc, lateral hypotarsal crest; lis, lateral intermetatarsal sulcus; lm, lateral margin; lt, lateral (hypotarsal) tuberosity; ltm, left tarsometatarsus; lvf, lateral vascular foramen; m2-4, metatarsal 2-4; mc, medial cotyle; mhc, medial hypotarsal crest; mis, medial intermetatarsal sulcus; mm, medial margin; mvf, medial vascular foramen; ns, neurovascular sulcus; ota, origin surface for toe abductor; p2-4, phalanx 2-4; pu, ungual (terminal) phalanx; rtm, right tarsometatarsus; sd, supratrochlear depression; ta, tarsus; t2-4, trochlea 2-4. Asterisks denote comparative material. Scale bar equals 1 cm.

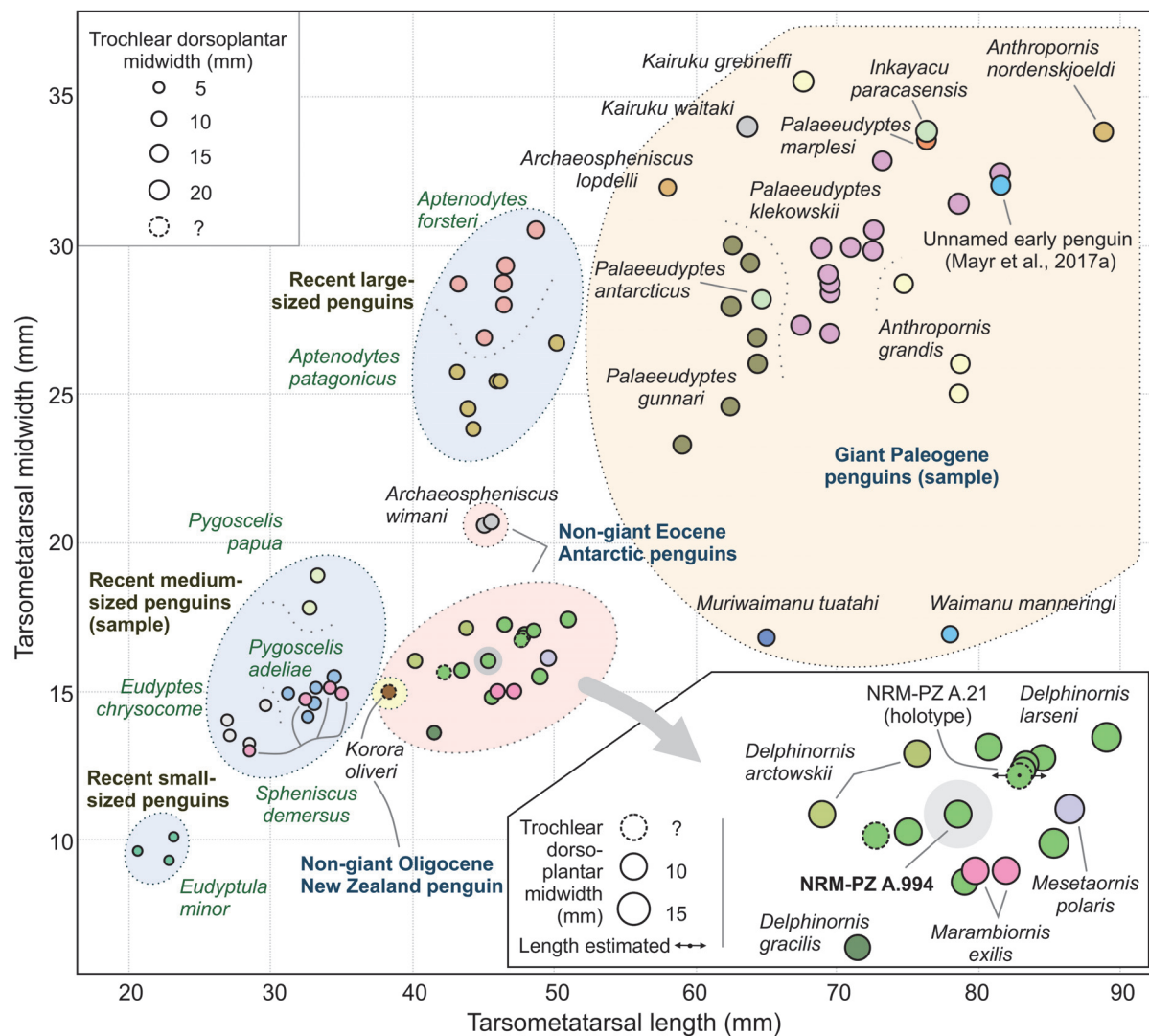
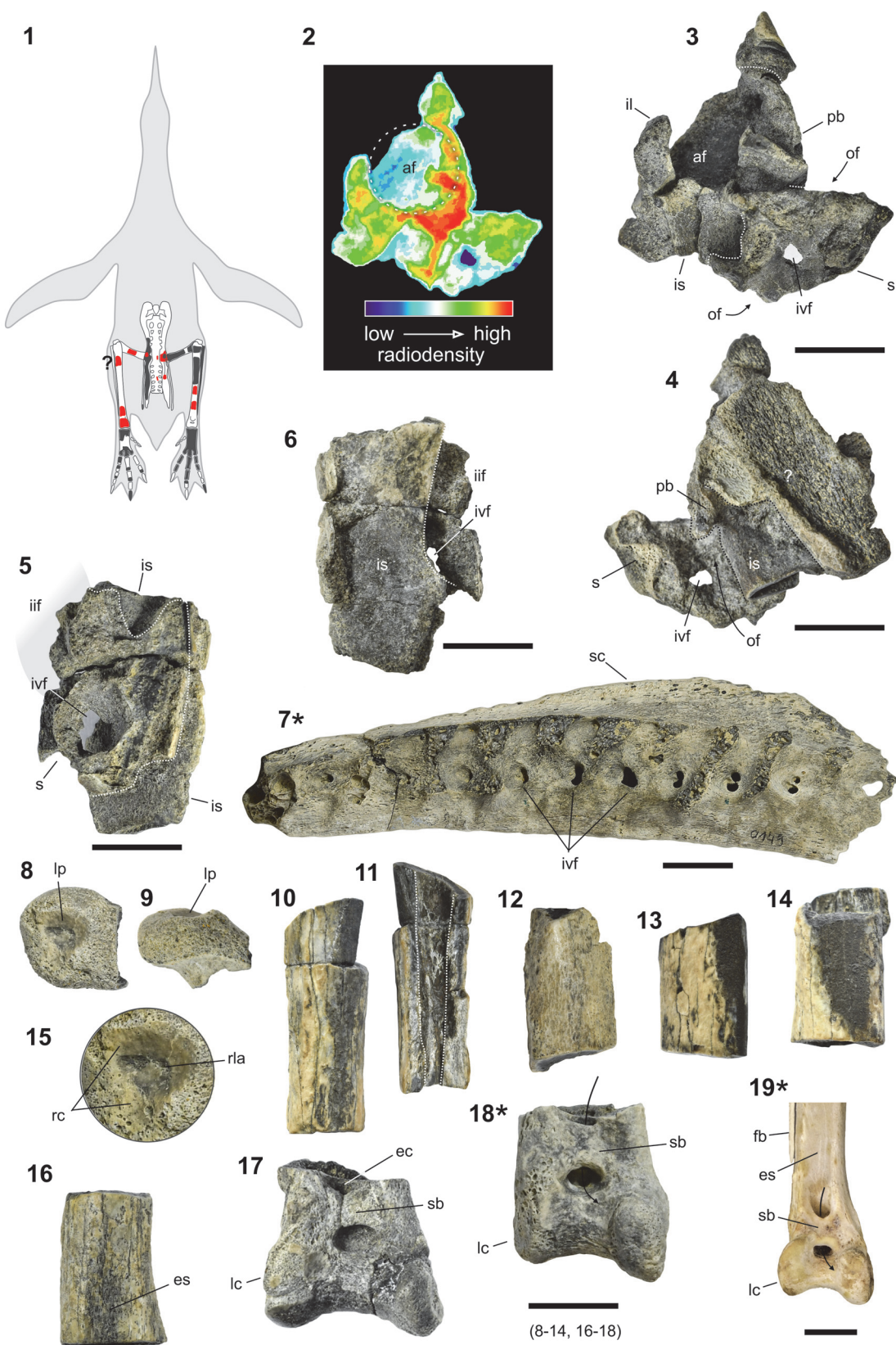


FIGURE 3. Comparison of tarsometatarsal measurements of selected present-day and Eocene penguins. The specimen maximum length and mediolateral midwidth are visualized as coordinates of a circle, whereas the dorsoplantar midwidth of the third trochlea - as its size. For specimen IDs, see Appendix 1.

penguins (e.g., Stephan, 1979, figure 41), even within the genus (pers. obs., based on unnumbered modern-pygoscelid specimens from IB/P/B). Considering the antitrochanteric inflection in the above genus of medium-sized Sphenisciformes, NRM-PZ A.994 resembles *P. papua* most.

The ilioischadic foramen is much larger than the acetabular opening, oval (which is clear, despite the incomplete iliac margin), with its major axis clearly longer than the minor one (30.4 mm vs. 14.1 mm). In this regard, the new specimen resembles other early Sphenisciformes, especially Paleocene *Waimanu manneringi* (Slack et al., 2006, figure 1.A) and unassigned Eocene IB/P/B-0488 (Figure 5.10-11) as well as even some extant

volant aquatic birds, e.g., loons and albatrosses (Wilcox, 1952, figure 11; Klemm, 1969, figure 38; see also Ibáñez and Tambussi, 2012, figure 1). The opposite part of the spectrum includes, among others, Miocene *Madrynornis mirandus* Acosta Hospitaleche et al., 2007 (early crown penguin; Acosta Hospitaleche et al., 2007, figure 5.B) and modern penguins (e.g., Figure 5.7, 5.12; Zusi, 1975, figure 4.1; we discuss it later in our work). In Plotopteridae, extinct penguin-like seabirds from the Northern Hemisphere, the ilioischadic foramen, albeit large, is clearly tapered cranially (unlike in penguins; Mayr and Goedert, 2018, figure 3.B-C, 3.F). In the majority of present-day birds, said opening is roughly round or short oval (Baumel and Witmer,

**FIGURE 4** caption next page.

1993). The major axis of the oval (which is common in birds; Baumel and Witmer, 1993) obturator foramen is ca. 10.8 mm long and devoid of a large portion of its ventral pubic margin. The ischiadic attachment site for the ischiopubic ligament is spindle-shaped (like in Eocene IB/P/B-0488, subcircular in pygoscelids; Figure 5.9, 5.11-12).

The body of the ischium is characteristically angular in medial view (Figure 5.4). The wider, medial surface of the cranial ischium and its virtually ventral counterpart meet at right angles and the resulting edge is parallel to the main axis of the hip bone. Such a sharply defined angularity appears to be not traceable in present-day penguins (Figure 5.12), but it is conspicuous in Eocene IB/P/B-0488 and IB/P/B-0627; Figure 5.10). The caudal extension of the ilioischiatric pillar, a bony reinforcing structure, is clearly visible, due to surface damage to adjacent fossilized tissue, along the postnatal ankylosis between two main coxal constituent parts (Figure 5.4). Both, the preserved postacetabular ilium and available fragments of the ischiadic wing appear to be rather delicately built, especially their off-axial surfaces. Their joint surface is smoothly convex medially. Retained fragments suggest relative elongation of the postacetabular pelvis. The length of the preserved ilioischiatric part of the postacetabular region, which most likely underestimates the actual dimension, exceeds five and a half acetabular diameters (medial view; Figure 5.2, 5.4). Taking into account the above note, this indicates more pronounced elongation than in complete extant specimens used for Figure 6 (see also Appendix 1), most of them do not exceed the value of five diameters. Relatively elongated postacetabular hip bone appears to be present in Oligocene *Kairuku greb-*

neffi (Ksepka et al., 2012, figure 6.D-F), and more so in some volant aquatic birds (Ibáñez and Tambussi, 2012, figure 1). In the case of fossils, however, their incompleteness precludes certainty in this respect.

The medial surface of the preacetabular ilium has a conspicuous (though shallow) facet for articulation with the transverse process of a sacral vertebra (Figure 5.4). Such a scar has been previously documented by Clarke et al. (2003, figure 4.B; see also Acosta-Hospitalche and Olivero, 2016, figure 4.A) for another Eocene hip bone (not articulated with sacrum). This is a part of an incomplete skeleton from Tierra del Fuego (Argentina), recently assigned to *Palaeudyptes gunnari* (see Acosta-Hospitalche and Olivero, 2016). The facet is also present in a relatively small-sized Eocene specimen IB/P/B-0211 (Figure 5.5) and large IB/P/B-0488 (Figure 5.10), and is common in present-day penguins (pers. obs.). Another preserved surface for contact with the sacrum is represented by a short fragment of the iliac part of the iliosacral suture located between the acetabulum and ilioischiatric foramen (Figure 5.4, 5.8). The right hip bone is partially covered by matrix together with three left leg bones: the femur, tibiotarsus, and fibula (Figure 5.2-4, 5.6).

Femora. The incomplete left femur comprises the poorly preserved head and proximal shaft, well-preserved diaphyseal midsection and damaged distal end with condyles. It is ca. 91.0 mm long, a distance measured between the ligament fovea of the head and medial condyle. The overall length of the bone is comparable to that of the largest individuals of *Pygoscelis papua* and some representatives of *Aptenodytes patagonicus* (pers. obs.; Stephan, 1979, table 1). It is clearly larger than IB/

FIGURE 4 (continued from previous page). Minor fragments of pelvic skeleton and leg bones of Eocene *Delphinornis larseni*, NRM-PZ A.994. 1. Location of these skeletal elements within penguin body, in ventral view, is presented in red. Other bones included in NRM-PZ A.994, and shown in Figures 2.1-7, 2.15, 2.17-19, 5.3-4, 5.6, 5.8-9, 5.13, 5.16, are in gray. 2. Heat map of left acetabular socket, based on X-ray. 3. Left acetabular socket in medial view with associated portion of sacrum. 4. Same in lateral view with exposed cranial frame of obturator foramen. 5. Left ischium in medial view with associated portion of sacrum. 6. Same in lateral view with exposed fragment of caudal frame of ilioischiatric foramen. 7. Right-side view of Eocene sacrum IB/P/B-0149 (Eocene, Seymour Island, Antarctica). 8. Right femoral head in proximal view. 9. Same in caudal view. 10. Middle shaft of right femur (undetermined aspect of preserved wall). 11. Same in opposite view, showing pronounced stricture of medullary cavity. 12. Alleged fragment of proximal shaft of right tibiotarsus. 13. Middle shaft of left tibiotarsus in cranial view. 14. Distal shaft of same in cranial view. 15. Right femoral head in proximal view - close-up of ligamental pit. 16. Distal shaft of right tibiotarsus in cranial view. 17. Distal end of same in cranial view. 18. Distal end of left Eocene tibiotarsus IB/P/B-1033 (Eocene, Seymour Island, Antarctica), reversed. 19. Distal fragment of left (reversed) tibiotarsus of extant *Pygoscelis papua* (NHMUK/T 1900.8.17.1). Abbreviations: af, acetabular foramen; ec, extensor canal; es, extensor sulcus; fb, fibula; iif, ilioischiatric foramen; il, ilium; is, ischium; ivf, intervertebral foramen; lc, lateral condyle; lp, ligamental pit; of, obturator foramen; pb, pubis; s, sacrum; rc, receptacle zone; rla, round ligament (one of its bundles) attachment point; sb, supratendinal bridge; sc, spinous crest of sacrum. Asterisks denote comparative material. Scale bar equals 1 cm.

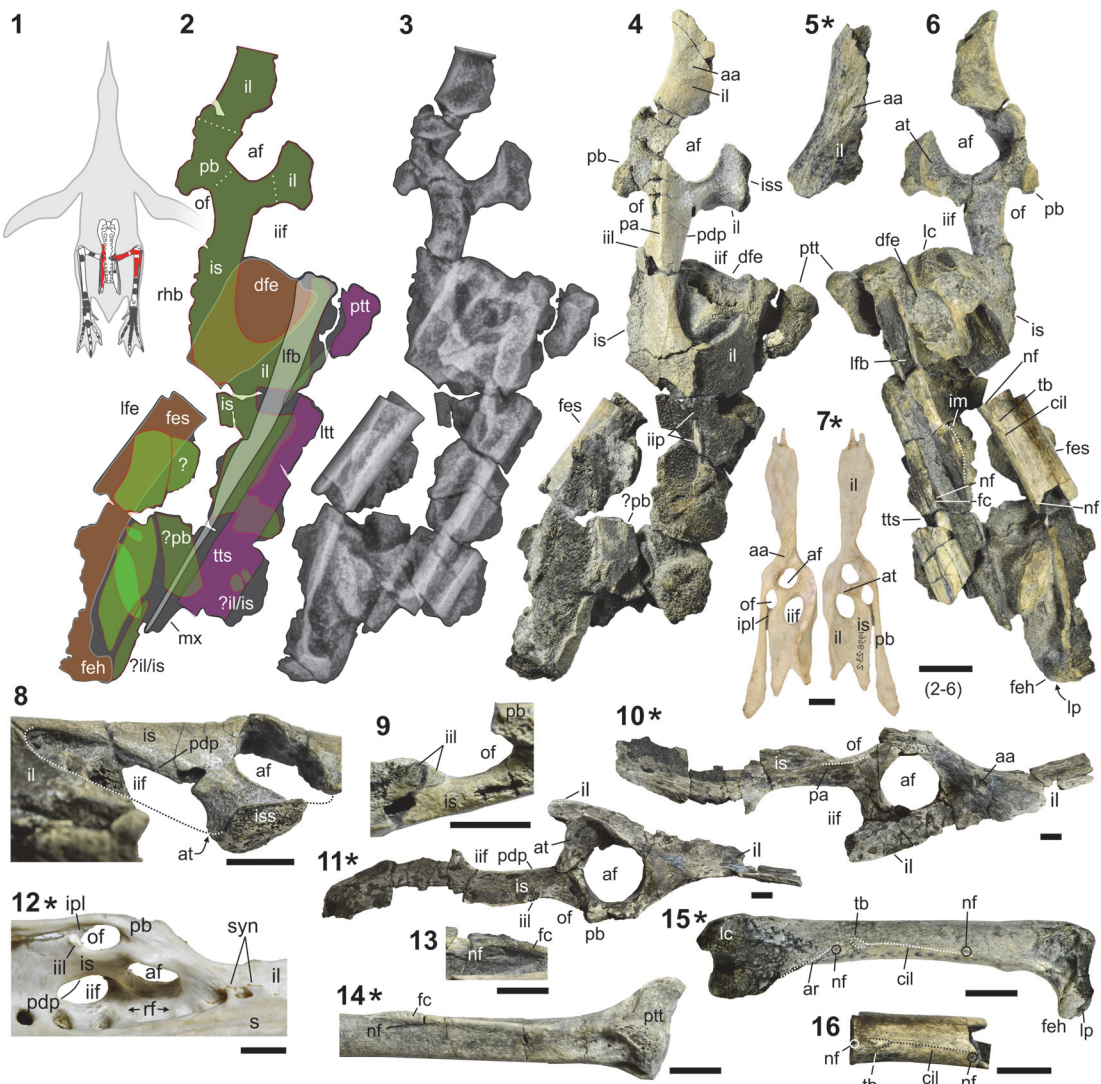


FIGURE 5. Incomplete pelvic skeleton and fragmentary leg bones of Eocene *Delphinornis larseni*, NRM-PZ A.994, major fragment (bones encased in a single lump of matrix). 1. Location of these skeletal elements within penguin body, in ventral view, is presented in red. Other bones included in NRM-PZ A.994, and shown in Figures 2.1-7, 2.15, 2.17-19, 4.2-6, 4.8-17, are in gray. 2. X-ray-based schematic view of right hip bone and associated left leg bones, as preserved in matrix. 3. X-ray image of same. 4. Medial view of same. 5. Fragmentary right preacetabular ilium IB/P/B-0211 (Eocene, Seymour Island, Antarctica) in medial view. 6. Lateral view of right hip bone and associated left leg bones (NRM-PZ A.994). 7. Right (reversed left) hip bone of extant *Spheniscus demersus* (Linnaeus, 1758), NHMUK/T S/1998.23.2, in medial (left) and lateral view. 8. Dorsomedial view of two major hip-bone foramina of NRM-PZ A.994. 9. Ventromedial view of obturator foramen of same specimen. 10. Medial view of right hip bone, IB/P/B-0488 (Eocene, Seymour Island, Antarctica). 11. Lateral view of same. 12. Ventromedial view of three major hip-bone foramina of extant *Pygoscelis papua* (unnumbered specimen from IB/P/B). 13. Dorsomedial view of nutrition foramen of left tibiotarsus (NRM-PZ A.994). 14. Same view of tibiotarsus IB/P/B-1033 (Eocene, Seymour Island, Antarctica). 15. Caudal view of reversed right femur IB/P/B-0130 (Eocene, Seymour Island, Antarctica). 16. Same view of middle shaft of NRM-PZ A.994. Abbreviations: aa, articular area; af, acetabular foramen; ar, adductor ridge; at, antitrochanter; cil, caudal intermuscular line; dfe, distal end of femur; fc, fibular crest; feh, femoral head; fes, femoral shaft; iif, ilioischiadid foramen; ill, insertion site for ischiopubic ligament; iss, ilioischiadid suture; lc, lateral condyle; lfb, left fibula; lfe, left femur; ltt, left tibiotarsus; lp, ligamental pit; mx, matrix; nf, nutrition foramen; of, obturator foramen; pa, pronounced angularity within ischium; pb, pubis; pdp, correlate of proximal dorsal process; ptt, proximal end of tibiotarsus; rf, renal fossa; rhb, right hip bone; s, synsacrum; syn, iliosynsacral synostosis; tb, tubercle; tbs, tibiotarsal shaft. Asterisks denote comparative material. Scale bar equals 1 cm.

P/B-0130 (Figure 5.15; Jadwiszczak, 2006, figure 14.A-B; hypothesized to represent *Delphinornis gracilis*) and slightly shorter than IB/P/B-0215 (Jadwiszczak, 2006, figure 16.A-B; hypothesized to represent *Mesetaornis polaris* Myrcha et al., 2002). Unlike the left head, its right counterpart (Figure 4.8-9), found in close vicinity, is in a good condition being the only proximal remnant of the respective bone. It is 11.4 mm wide and has a large proximal pit (the capital ligamental fossa/fovea), a round ligament insertion site. The pit consists of two distinct parts, a deeper, ovoid central area with a partially rough, darker floor and a peripheral zone with a smooth surface (Figure 4.15). The ligamental fossa is located (like in all but one Sphenisciformes and closely related Procellariiformes) medioproximally to proximally. In this respect, the only exception (medial placement) appears to be Paleocene *Crossvallia unienwillia* Tambussi et al., 2005, the poorly preserved Antarctic stem penguin (Jadwiszczak et al., 2013, figure 6.2-3, 6.5). The right femoral shaft is characterized by a well-defined curvature (similarly to *P. papua*, but unlike most other members of the Sphenisciformes; e.g., Figure 5.15; Ksepka and Clarke, 2010) and caudal intermuscular line that ends distally with a conspicuous tubercle (Figure 5.6, 5.16; not as prominent as in *Inkayacu paracasensis*; Clarke et al., 2010, figure 1.K). Clearly, there is an actual discontinuity between the above line and adductor ridge (Figure 5.16). Such a feature can be also observed in some other fossil penguin femora from the Eocene of Antarctica, both small- (e.g., IB/P/B-0130; Figure 5.15) and large-sized (e.g., IB/P/B-0108; unfigured), supposedly in Paleocene *Sequiwaimanu rosiaeae* Mayr et al., 2018 from New Zealand (Mayr et al., 2018, figure 11.A) as well as in *Paraptenodytes antarcticus* (Moreno and Mercerat, 1891) - a Miocene stem penguin from Patagonia (Bertelli et al., 2006, figure 19.D). Moreover, this discontinuity is quite conspicuous in present-day *Aptenodytes forsteri* and *A. patagonicus* (pers. obs., based on NHMUK/T S/1998.55.2 and NHMUK/T S/1846.4.15.31, to name two). The diaphyseal mid-section is essentially circular with its minimum mediolateral width of 8.8 mm (slightly wider than IB/P/B-0130 and narrower than IB/P/B-0215; Jadwiszczak, 2006, figure 16.A-B). Taking into account the minimal shaft diameter and head breadth, their values for NRM-PZ A.994 do not exceed those obtained from femora attributable to *P. papua* (pers. obs.; Stephan, 1979, table 1). Internally, it is characterized by a pronounced local narrowing of the medullary cavity, apparent on the X-ray image

(Figure 5.3). There are also two small matching shaft-wall fragments most likely of the right femur (Figure 4.10-11), assignable to the same individual, showing such a stricture (Figure 4.11). Proximally to the narrowing, the former shaft exhibits a small nutrient foramen, its opening slightly medial to the caudal intermuscular line. Another, even smaller foramen opens distally to the aforementioned line (Figure 5.6, 5.16). Both foramina are 21.5 mm apart. The proximal foramen, likely representing the entry point of the main nutrient artery (see Midtgård, 1982), is quite easily traceable (unlike the distal one) in modern and some Eocene penguin femora (e.g., Figure 5.15; see also Acosta Hospitaleche and Olivero, 2016, figure 4.D; Mayr et al., 2018, figure 11.A).

Tibiotarsi. The left tibiotarsus is poorly preserved (Figure 5.6), and its overall length cannot be reliably estimated. Its proximal part is represented by lateral and medial articular surfaces and a small remnant of the adjacent diaphysis. Distally, a much longer (48.3 mm) non-adjoining fragment of tibiotarsal diaphysis is present. It is relatively complete solely in its distal part, whereas the bulk of the preserved shaft is limited to the caudal surface with a partial fibular crest. The crest is accompanied by a short furrow leading to a small nutrient foramen (Figure 5.6, 5.13) - a common feature in Eocene penguins of different sizes (e.g., Figure 5.14), also present in present-day Sphenisciformes (distinctness varies; pers. obs.), Paleocene *Waimanu manningi* (Mayr et al., 2018, figure 11.H), and Oligocene *Kairuku grebneffi* (Ksepka et al., 2012, figure 7.D). The estimated diaphyseal mediolateral width just distal to the foramen is ca. 9.3 mm. Two isolated fragments of a more distal shaft section are most likely also, based on their cross-sectional shape, assignable to this bone (Figure 4.13, 4.14). The distalmost tibiotarsus is represented by two fragments from the right-limb skeleton: a fragmentary shaft showing a proximal part of the extensor sulcus (Figure 4.16) and, clearly non-adjoining, distal end with the supratendinal bridge, extensor canal, and condyles (Figure 4.17). The canal appears to be rather tight proximally (in comparison to some other similarly-sized Eocene bones, e.g., IB/P/B-1033; Figure 4.18), but the bridge appears to be fractured (Figure 4.17), which could affect the underlying tendinal passage. The bridge is moderately wide, narrower than in Miocene *Paraptenodytes antarcticus* (Bertelli et al., 2006, figure 20.C) and *Madrynornis mirandus* (Acosta Hospitaleche et al., 2007, figure 5.A) as well as extant *Pygoscelis papua* (Figure 4.19). The distal

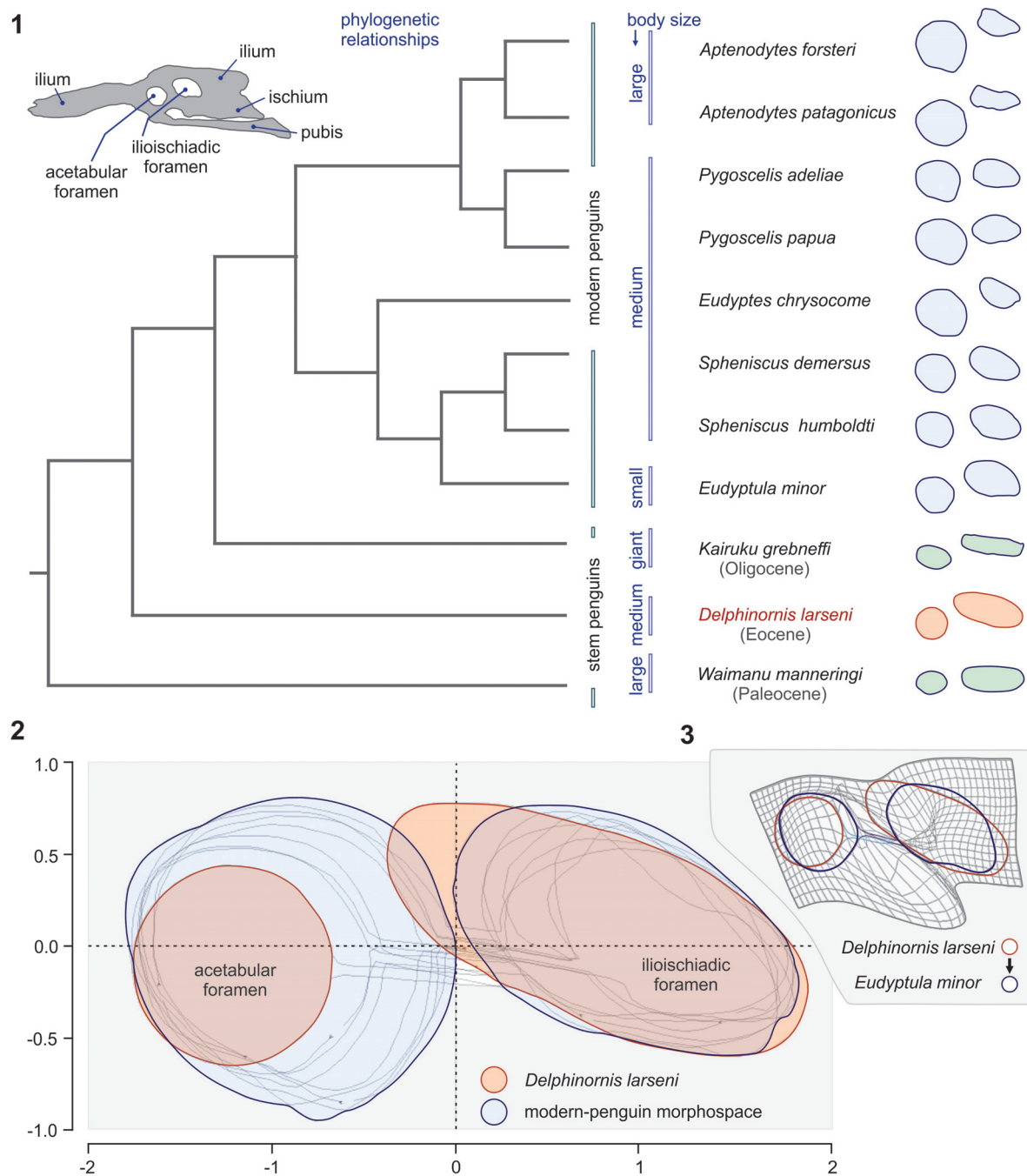


FIGURE 6. Shape analyses of outlines of major hip bone foramina. 1. Comparison of foramen configurations and shapes of eight extant and three stem-group penguins, including the Eocene specimen NRM-PZ A.994 (*Delphinornis larseni*); foramen pairs are not to scale, branching pattern for present-day species used in the cladogram follows Subramanian et al. (2013, figure 1). 2. Position of NRM-PZ A.994 relative to the extant-penguin morphospace, based on aligned, centered and scaled outlines. 3. Deformation grid between configurations representing NRM-PZ A.994 (*D. larseni*) and NHMUK/T S/2002.2.1 (extant *Eudyptula minor*). For other specimen IDs, see Appendix 1; for PCA plots, see Appendix 4.

opening of the passage is located centrally in relation to the condyles (Figure 4.17), unlike in Paleocene penguins (*Sequiwaimanu rosieae* and *W. manneringi*; Mayr et al., 2018, figure 11.J, 11.M). The medial condyle is ca. 18.1 mm wide caudocranially, whereas the mediolateral width of the whole fragment, measured between both condyles in distal view, amounts to ca. 17.9 mm. Considering the latter measurement together with the diaphyseal mediolateral width (see above), NRM-PZ A.994 most closely resembles IB/P/B-0266 (hypothesized to represent *Delphinornis arctowskii*; Jadwiszczak, 2006, table 20). The analyzed material also includes a single long-bone fragment, presumably representing (judging from its angular shape) a proximal tibiotarsal shaft (Figure 4.12).

Fibula. The left fibula, the only one available, is quite well preserved (Figure 5.6). It is 78.6 mm long and 8.8 mm wide proximally. The shaft gradually decreases in its width down to the level of the fibular crest of the collaterally located tibiotarsus, where it expands laterally. This expansion, constituting the insertion point for the iliofibular muscle (Baumel and Witmer, 1993, figure 4.17), is sharper defined than in modern penguins (pers. obs.; Stephan, 1979, figure 47.1), and apparently also in *Palaeudyptes gunnari* (Acosta Hospitaleche and Reguero, 2010, figure 4.G) and *Kairuku grebneffi* (Ksepka et al., 2012, figure 7.B). A distalmost one-third of this bone is very thin.

Tarsometatarsi. The complete left tarsometatarsus and six associated pedal phalanges have been originally located within the same lump of matrix (Figure 2.18). Bones have been in close contact, though largely displaced. The tarsometatarsus (Figure 2.2-7) is relatively elongated like many early penguins (e.g., Myrcha et al., 2002; maximum length of 45.4 mm, 44.1 mm along main axis – to the groove of the third trochlea, midwidth of 16.0 mm) and flattened dorsoplantarly (the latter is typical of all penguins; e.g., Figure 2.20-21; Stephan, 1979; Myrcha et al., 2002). The third metatarsal is 6.4 mm thick in its midsection. This bone is smaller than most well-preserved specimens attributable to *D. larseni*, including the holotype (for more contrasts, see Figure 3). The comparative and functional aspects of tarsometatarsal elongation are considered in Discussion and Conclusions. The location of fusion between three ankylosed metatarsals and the distal tarsal bone is well marked internally, the condition revealed by the X-ray imaging (Figure 2.18). Externally, the markings are constricted to a low dorsal crest – a partial distal frame of the infracotylar fossa, and

proximal swelling of the medial margin of the bone (Figure 2.2). The wide oval medial cotyle is strongly concave, whereas its lateral counterpart resembles a clearly narrower flat shelf. The intercotylar eminence (Figure 2.2) is distinctly less prominent than in Paleocene *Waimanu manneringi* (Slack et al., 2006, figure 1.C) and, in medial and lateral views (Figure 2.3-4), virtually level with the intercotylar area. The proximal part of the bone is 18.9 mm wide mediolaterally. The medial hypotarsal crest and lateral hypotarsal tuberosity (see below) are separated by the well-developed sulcus (Figure 2.5-6; much shallower in present-day penguins, but clearly deeper in Eocene *Marambiornis exilis* Myrcha et al., 2002 and Procellariiformes; Jadwiszczak, 2015, figure 6). The medial hypotarsal crest, in terms of its mediolateral width and cross-sectional shape, subtly resembles its equivalents in some more crownward penguins, e.g., Eocene *Anthropornis* sp. (not all specimens from this genus; Acosta Hospitaleche and Jadwiszczak, 2011, figure 3.B-C) and Miocene *Paraptenodytes antarcticus* (Bertelli et al., 2006, figure 21.C-D). The lateral hypotarsus is dominated by the lateral of intermediate crests. Its medial counterpart is barely visible along the proximal section of the former ridge; the proper lateral hypotarsal crest is vestigial as well. Nevertheless, the hypotarsus described above, together with its counterparts in congeners, appears not to be as simple as its counterparts in modern penguins (e.g., Jadwiszczak, 2015, figure 6.A, 6.D, 6.G, 6.J) and Oligocene *Kairuku* (Ksepka et al., 2012, figure 7.L, 7.P). The other extreme of the spectrum (i.e., notably distinct crests – like in most birds, including Procellariiformes; Baumel and Witmer, 1993; Jadwiszczak, 2015, figure 6) is represented by Paleocene (Mayr, 2017a, figure 1.C-D, 1.F, 1.H) and some Eocene Sphenisciformes (especially *Marambiornis exilis*; Myrcha et al., 2002, figure 15.B; Jadwiszczak, 2015, figure 6.I).

The fourth metatarsal is straight (Figure 2.2, 2.4-5; unlike in Oligocene *Archaeospheniscus loddelli* Marples, 1952, and *Dunroonornis parvus* Marples, 1952, from New Zealand; Marples, 1952, figure 8.3-4, 8.5; post-mortem deformation cannot be excluded), whereas the second one is distally slightly curved abaxially in dorsal view, just before the respective trochlea (Figure 2.2-3; not as much as in, e.g., *Palaeudyptes*; Myrcha et al., 2002, figures 7, 8). The dorsal surface of the third metatarsal is plantarly lowered in its proximal part. X-ray imaging revealed the pronounced localized narrowing of the medullary cavity in distal sections of

all three metatarsals (Figure 2.18). The insertion site of the tibial cranial muscle is fusiform in shape (Figure 2.2; wider, approximately oval in present-day and larger fossil penguins; Jadwiszczak, 2006, figure 5.A, 8.A, 2015, figure 4.A; Ksepka et al., 2012, figure 7.M, 7.Q; Mayr et al., 2017a, figure 1.A). Both proximal vascular foramina are small, like in Paleocene penguins (Slack et al., 2006, figure 1.A; Mayr et al., 2017a, figure 1.A) and Eocene *Marambiornis exilis* (Myrcha et al., 2002, figure 15.A), the lateral one is slightly more proximal (Figure 2.2; like in *M. exilis*; Myrcha et al., 2002, figure 15.A). Moreover, judging from the X-ray image (Figure 2.18), it appears to be a little better developed on the whole than the quite slit-like medial foramen, which is not that obvious during external examination. The medial foramen is medially framed by two convex impressions of the extensor retinaculum. Both plantar proximal openings are more or less abaxial relative to the hypotarsal sulcus and crests (Figure 2.5; like in most penguins, Paleogene exceptions are represented by *Marambiornis* and *Mesetaornis*; Myrcha et al., 2002, figures 13.B, 14.B, 15.B). The distal vascular foramen is present (a plesiomorphy; e.g., Mayr et al., 2017a), evidenced by both the X-ray (Figure 2.19) and plantar-aspect morphology of the lateral intertrochlear notch (Figure 2.5), but supposedly not fully enclosed. This plesiomorphic trait (e.g., Mayr et al., 2017a) is present in Paleocene (Slack et al., 2006, figure 1.A; Mayr et al., 2017a, figure 1.C) and relatively small-sized Eocene Antarctic penguins (its distinctness varies; see Myrcha et al., 2002). The medial intermetatarsal sulcus is slight, whereas its lateral counterpart is well formed (Figure 2.2; intensity of this asymmetry varies in stem penguins; e.g., Myrcha et al., 2002). These structures are barely traceable plantarly (Figure 2.5). The plantar supratrochlear depression is constricted to the distal third metatarsal (wider mediolaterally in *M. polaris*, shifted medially in *M. exilis*; pers. obs.; Myrcha et al., 2002, figure 13.B, 15.B). The third trochlea is the largest one (Figure 2.7), its dorsoplantar midwidth of 10.4 mm and maximum mediolateral width of 8.1 mm. The distal mediolateral width of the tarsometatarsus, measured between the midpoints of trochlear margins in distal view, amounts to 22.8 mm.

The right tarsometatarsus is represented by two isolated and non-adjoining fragments of proximal and distal parts with some portions of metatarsals attached (Figure 2.1). They are less well preserved than their left-sided counterparts. Most importantly, the latter specimen directly indicates

the presence of a dorsal opening of the distal vascular foramen.

Pedal phalanges. Digits of the left foot are represented by eight recognized phalanges, which are largely well preserved (Figure 2.17). The second digit retained a proximal and intermediate of its three phalanges, the third digit is devoid solely of the ungual phalanx and its penultimate (third) phalanx is very fragmentary, and within the five-unit-long fourth digit, two unambiguous proximalmost phalanges remained, most likely accompanied by the distalmost (ungual) bone. The first phalanx of the third digit, the largest unit within a penguin forefoot, is 29 mm long plantarly, measured along its main axis. The slender-built ungual phalanx of the fourth digit, devoid of its very apex, is 15.8 mm long plantarly. Both of its curved neurovascular sulci are present, the medial groove is much better developed and more dorsal. The flexor tubercle is prominent. Of all the aforementioned phalanges, only the second and third bones from the third digit were not encased by matrix together with the tarsometatarsus (Figure 2.18).

The right-foot toes are known from the first three incomplete phalanges of the fourth digit, the first two even more fragmentary phalanges of the third digit, supplemented by the well-preserved ungual unit, and a small fragment of the second phalanx from the second digit (Figure 2.15). The ungual bone has a slightly abraded proximal end and is devoid of a small portion of its distal tip. Nevertheless, it is stouter in appearance than the only known ultimate phalanx from the left foot, and its lateral neurovascular sulcus is also deeper and wider.

The associated phalanges that are assignable to a named genus or species are not common in the fossil record of early Sphenisciformes. The proximal phalanx of the third digit (i.e., the largest one) from NRM-PZ A.994 (Figure 2.17) is relatively more elongated (i.e., possesses larger midlength/midwidth ratio) than its counterpart in giant Eocene penguins from Antarctica: *Anthropornis* sp. (Jadwiszczak, 2012, figure 3.A) and *Palaeudyptes klekowskii* (Acosta Hospitaleche and Reguero, 2014, figure 7.L). In this respect, *Delphinornis larseni* resembles CM 2016.158.1, an unnamed giant penguin from the Paleocene Waipara Greensand in New Zealand (Mayr et al., 2017a, figure 1.A). The proximal phalanx from the second digit has similar proportions to that in *P. klekowskii* (Acosta Hospitaleche and Reguero, 2014, figure 7.M). The second phalanx of the third digit from NRM-PZ A.994 seems to be relatively more elongated than its

counterpart in another large-sized stem penguin, *Inkayacu paracasensis* from the Eocene of Peru (Clarke et al., 2010, figure S.3), but this difference is much smaller when compared with the Waipara Greensand penguin. Two proximalmost phalanges of the fourth digit from CM 2016.158.1 appear to be relatively more elongated than those in NRM-PZ A.994. The issue of phalangeal proportions is also considered in Discussion and Conclusions.

DISCUSSION AND CONCLUSIONS

The tarsometatarsus, due to the very nature of the fossil record of Antarctic penguins, has constituted the only element unambiguously assignable to *Delphinornis* (Simpson, 1971; Myrcha et al., 2002; Jadwiszczak, 2006). The proportions of the complete left bone, quite typical of the species (e.g., Figure 2.2, 2.8-9), clearly differ from their counterparts in extant penguins (e.g., Figure 2.20-21). Although discussed specimens are longer than some foot bones belonging to *Aptenodytes* Miller, 1778, the largest present-day Sphenisciformes, they are at the same time much thinner mediolaterally. Considering the latter dimension, NRM-PZ A.994 resembles some medium-sized extant penguins (Figure 3).

Relatively elongated tarsometatarsi are characteristic of all known Paleocene and many Eocene penguin species (Myrcha et al., 2002; Slack et al., 2006) as well as, much more pronouncedly, Procellariiformes (pers. obs.; Klemm 1969, figure 45) – the closest living relatives of extant penguins (e.g., Simpson, 1976; Hackett et al., 2008). Hence this is an obvious plesiomorphy. Recently, a conspicuous morphological disparity among Paleocene Sphenisciformes, also in terms of foot-bone proportions, has been reported by Mayr et al. (2017a). However, even the relatively shortened tarsometatarsus of an unnamed penguin from the mid-Paleocene of New Zealand (see Mayr et al., 2017a, figure 1) differs in this respect from its counterparts in crown-group Sphenisciformes or Spheniscidae sensu Clarke et al. (2003).

Tarsometatarsal elongation has its functional consequences, for instance, for the force output during ankle (intertarsal joint) flexion. Considering any group of geometrically similar birds, the longer the tarsometatarsus (outforce lever arm) relative to the distance between the flexor attachment and intertarsal joint, representing the inforce moment arm, the lower the magnitude of the force output (Zeffer and Norberg, 2003). The ratio of the latter to the former length, calculated for NRM-PZ A.994, amounts to 0.363. This value (hence also the rela-

tive force output) is slightly larger than the ratio in another well-preserved bone assignable to *Delphinornis larseni* (Figure 2.9-14; 0.351) as well as type specimens of *D. arctowskii*, *D. gracilis*, and *Marambiornis exilis* (0.341, 0.351, and 0.334, respectively), all of them from the Eocene. However, it is slightly smaller than that of another Eocene penguin – *Mesetaornis polaris* (0.371) and more so relative to extant pygoscelid penguins (>0.4).

Present-day penguins, like most birds, are essentially digitigrade; i.e., they walk on their toes, although use whole feet at rest (pers. obs.; see also Simpson, 1946). It is most parsimonious to assume that they share this trait with their Paleogene relatives. This view has recently gained support by the observation that the alleged lumbosacral sense organ for the control of walking (Necker, 2006) does not differ substantially between the Eocene and extant Sphenisciformes (Jadwiszczak, 2014).

Distal width of the largest foot bone, the tarsometatarsus, constitutes a proxy for the span of extreme proximal-phalanx bases. In this regard, the NRM-PZ A.994 is within the range of values reported by Stephan (1979, table 1) for the extant Gentoo penguins, *Pygoscelis papua*, the largest among medium-sized modern Sphenisciformes (see Williams 1995). Interestingly, two proximalmost phalanges from each of three main digits (well preserved in the fossil skeleton) are clearly longer (and more elongated) in the Eocene specimen (Figure 2.15, 2.17). Additionally, the elongated tarsometatarsus can provide larger surface areas for the origins of toe abductors, muscles that arise fleshy from the second and fourth metatarsals in present-day penguins (Schreiweis, 1982; Jadwiszczak, 2015, figures 4, 5). One of such enlarged areas (related to the abductor of the fourth digit) is especially well delineated in IB/P/B-0547, another specimen assignable to *D. larseni* (Figure 2.8).

Considering condition of the abductor of the fourth digit, there is some variation among Procellariiformes. In this sister clade/taxon (characterized by much longer fore- and hindfoot bones), the muscle can be fleshy proximally and distally (i.e., with two origins, tendinous within the middle third; albatrosses) or fleshy along its length (shearwaters), or even originate distally (storm petrels; Klemm, 1969). The abduction produced in the first scenario was specified by Klemm (1969) as strong.

The above findings indicate the longer forefoot and theoretically wider toe spacing attainable by *Delphinornis larseni*. Such a characteristic

potentially facilitates, by spreading body weight over a wider area, walking by reducing the risk of losing balance. The said condition, together with the elongate tarsometatarsus (e.g., Figure 2.2, 2.9), obviously leads to larger hydrodynamic drag. On the other hand, penguins are wing-propelled divers, using their feet as a rudder. To enlarge its area, extant (i.e., short-footed) Sphenisciformes possess additional dermal flanges on foot sides (Figure 2.16; Cornthwaite, 2013), an adaptation possibly either not present or not that essential for at least some early penguins. Moreover, like the vast majority of marine birds, penguins and their closest living relatives (Procellariiformes) have webbed feet (e.g., Schreiber and Burger, 2002). The members of the latter group, however, do not possess additional dermal flanges (pers. obs.). Those of them that dive, use their wings as oars, just like penguins (e.g., Del Hoyo et al., 1992).

The proximal fovea of the right femoral head (Figure 4.8-9, 4.15) has a heterogeneously formed floor with the ovoid central area, constituting the actual attachment site of the round ligament of the femur. The smoother and shallower peripheral area apparently (partly) served as a receptacle zone (e.g., Perumal et al., 2017). The fovea reveals an osteological aspect of the bone-ligament interface – a distribution of units reflecting higher contact intensity (separate bundles) (Figure 4.15). They are distinguishable by differences in their tinge, depth, and presence of foramina, at least some of them being vascular. No other femoral fovea in available fossil-penguin specimens represents such a degree of detail.

The pelvis of early penguins, including NRM-PZ A.994, exhibits a well-defined fixed asymmetry in the size of two main hip bone openings, the acetabular foramen being always smaller than the ilioischiatric foramen (Figure 6; see also Jadwiszczak 2006, figure 19). Extant penguins are clearly more diversified in this respect (Figure 6.1-2), the former condition present within the *Eudyptula-Spheniscus* group (Figure 6.1; Zusi, 1975). The configuration exhibited by *Delphinornis larseni* is most closely approached by much smaller *Eudyptula minor* (Forster, 1781). However, even in this case, differences are obvious (Figure 6.3). The large and elongated ilioischiatric foramen of Paleogene Sphenisciformes (Figure 6.1) supposedly represents an ancestral trait state, because it is also larger than the acetabulum and often clearly elongated in Procellariiformes (e.g., Klemm, 1969; Mayr, 2009). The oldest penguins exhibiting inverse proportions of opening sizes are known

from the Miocene (e.g., Acosta Hospitaleche et al., 2007, figure 5.B).

In birds, the cranial part of the ilioischiatric foramen transmits the ischiadic nerves and vessels, the remaining part of the opening is occupied by the connective tissue sheet (a membrane), with muscles attached to its both surfaces (Baumel and Raikow, 1993). Hutchinson (2001) claimed that the proximal dorsal process of the avian ischium is correlated with the formation of the above membrane. If so, then the characteristic point-of-change of the ischiadic-rim width, observable in at least some penguin fossils (NRM-PZ A.994, but also in large IB/P/B-0488; Figure 5.8, 5.11) and modern bones (Figure 5.12), that in our estimation corresponds to that process, marks the proximalmost attachment of the membrane (see also Hutchinson, 2001). Assuming correctness of our reasoning, the unobstructed area of the ilioischiatric foramen accounted for about a third of the entire opening in Eocene sphenisciforms. Such a fraction is typical of most birds (see Baumel and Raikow, 1993), but not necessarily of present-day penguins. In the latter group, the above-mentioned point is located closer to the caudal frame (Figure 5.12; Appendix 5), hence the membrane covers a smaller part of the opening (Appendix 5).

According to Midtgård (1982), in extant penguins (represented in his study by *Spheniscus humboldti* Meyen, 1834), unlike in a majority of birds (including Procellariiformes), the ischiadic artery is not the main blood vessel supplying most of the hind limb. If there was a link between reducing the size of the ilioischiatric foramen during penguin evolution (see Figure 6) and gaining the importance by the femoral artery, a vessel not associated with the above foramen, the early Sphenisciformes might have been more like procellariiforms in this regard.

The above shrinkage was possibly related to the ossification of the ilioischiatric membrane resulting from the assumed shortening/reinforcement of the postacetabular pelvis (see comparative description of hip bones) and associated (hypothetical) craniad shift or expansion of origins of relevant muscles, e.g., the ischiofemoral muscle. The origin of this flexor is caudal to the ilioischiatric foramen and its origin in modern penguins is “extensive” (Schreiweis, 1982, figure 41). Both in turn could have been connected to the evolution of the streamlined form (useful when diving) with legs shifted backwards, enforcing a (fully) upright posture on land (including use of shorter tarsometatarsi; in water, feet essentially serving as a rudder).

Another factor, that ought to be taken into account, is a possible selection for the better protection (by shrinking “holes”) of the caudal portion of kidneys, especially during deep dives.

The spin-off of that evolutionary process could have been a higher risk of choke-point formation (see Wideman, 2016, figure 6), resulting in an increased incidence of complications such as aneurysm and ischaemia. Assuming the above scenario, increasing the importance of the femoral artery would be advantageous. Although the persistence of an ancestral character state in stem penguins appears to be plausible, the issue flagged up here requires further studies.

Penguins, typically of seabirds, are long-lived and banding records indicate that some individuals can live much longer than 20 years, and even breed after crossing their twenties (e.g., Dann et al., 2005). Results of our analysis of the specimen NRM-PZ A.994 indicate that the individual discussed here was most likely a relatively young bird. We surmise that the above penguin was up to several years old; decidedly not a chick, because the fusion of tarsometatarsal components is outwardly complete (Figure 2.2-5). Against the really advanced age of the individual testify the following foot-bone conditions: the presence of very slight traces of plantar intermetatarsal sulci (especially the lateral one; Figure 2.5), transition between the second metatarsal and tarsus marked as an abrupt bone swelling (Figure 2.2-3), the whole synostosis zone between proximal metatarsals and the tarsal component conspicuous internally (highly radiopaque; no “cross-border” remodeling marked; Figure 2.18). Moreover, the distal vascular foramen was possibly not as well developed as that in the holotype and some other tarsometatarsi attributable to *D. larseni* (e.g., Figure 2.8-9). In this case, we admit we cannot completely rule out the influence of post-mortem factors.

Another indication of the relatively young age of the studied individual is seen on the medial surface of the preacetabular ilium. Skeletons of mature birds are most often characterized by the fusion of the ilium and sacrum. This is manifested, among others, by synostoses formed between vertebral transverse processes and the neighboring areas of the iliac surface (Baumel and Witmer, 1993). Such an age-dependent tendency is more or less traceable in extant Sphenisciformes and is especially pronounced in pygoscelid penguins (e.g., Figure 5.12). A single process/ilium contact area is visible in the Eocene specimen NRM-PZ A.994 (Figure 5.4). Its form (an articular

cotyle) and texture in the fossil bone preclude the complete fusion, rather being suggestive of a less rigid connection. In contrast to NRM-PZ A.994, another fragmentary ilium from the Eocene of Seymour Island (IB/P/B-0211; Figure 5.5), an isolated element belonging to a slightly larger individual from unknown species, possesses a smaller cotyle with much smoother surface. In our estimation, this difference reflects the actual condition – a less definite element connection in the latter bird. Moreover, such a cotyle is also present in some other giant penguins (see comparative description of hip bones), whereas more definite connections can be observed in the giant penguin genus *Kairuku* (Ksepka et al., 2012, 6.C, 6.F). Interestingly, the preserved iliac part of the iliosynsacral suture in NRM-PZ A.994 (Figure 5.6, 5.8) is very rough, indicating a fracture within rigidly united elements, therefore precluding a very young age of the bird.

According to Jadwiszczak and Chapman (2011, figure 1), rough estimates obtained by Jadwiszczak (2001) via the modelling of the tarsometatarsal dorsoplantar width and overall body length relationship, suggest that small individuals assignable to *D. larseni*, and NRM-PZ A.994 is not that large, could have been slightly shorter than some extant Gentoo penguins, *Pygoscelis papua*. Considering longer weight-bearing bones, femoral shaft and head dimensions are often utilized in body-mass assessments (e.g., Brassey, 2016). Taking cognizance of femoral dimensions, the studied skeleton belonged to an individual both shorter and lighter than whichever representative of so-called giant penguins (e.g., Jadwiszczak and Chapman, 2011) from the Eocene of Seymour Island.

Since its first formal description (Wiman, 1905), *D. larseni* has remained quite an enigmatic bird with its hypodigm expanding throughout the inclusion of further tarsometatarsi. Whereas giant early Sphenisciformes, in a sense, ruled the minds of researchers studying the evolutionary history of this fascinating order of birds, fueled by the growing number of discovered skeletons, the fossil record of smaller-sized stem-group penguins has been gaining rather quantitatively than qualitatively. The specimen reported here is a game-changer in paleontology of stem penguins, offering insight into valuable details of the pelvic girdle and hind-limb bones of the latter group and hopefully reducing the existing bias towards the larger birds.

We currently know that modest-sized Eocene penguins assignable to *D. larseni* were osteologically “slender-footed” in respect to both (tarsometatarsal

tarsal and digital) distalmost components of the hind limb. Their postacetabular hip bones (precisely - their main, ilioischadic parts, which are much better preserved than preacetabular ones) were apparently relatively elongated, possessing the extensive ilioischadic foramen, largely covered with membrane. These major findings, unique for non-giant stem penguins, supplemented by a number of other observations, contribute to the known set of character configurations. Hence our report can have obvious uses in prospective refinements of published cladograms. The functional angle appears to be indispensable as well. It ranges across well-grounded considerations (the force output during intertarsal joint flexion), those slightly debatable (the role of elongated toes in reducing the risk of losing balance on land), and more speculative (though logically justified – increasing the importance of the femoral artery). Although we consider our contribution as an important step forward in penguin paleontology, the catchphrase “more research is needed” remains appropriate.

ACKNOWLEDGMENTS

The authors would like to thank the editors for considering the manuscript and two anonymous reviewers for their constructive and insightful comments. PJ acknowledges the financial support through SYNTHESYS funding made available by the European Community – Research Infrastructure Action under the FP7 Structuring the European Research Area Programme; projects GB-TAF-987 and GB-TAF-4610. TM thanks the Argentine Antarctic Institute (IAA-DNA), especially M. Reguero and the Argentine Air Force for logistical fieldwork support including the great hospitality at the Marambio Base as well as the Swedish Polar Research Secretariat (SPFS) for logistical support. J. Moly and J. O’Gorman are thanked for assistance in the field. Financial support from the Swedish Research Council (VR Grant 2009-4447) is gratefully acknowledged.

REFERENCES

- Acosta Hospitaleche, C., Hagström, J., Reguero, M., and Mörs, T. 2017a. Historical perspective of Otto Nordenskjöld's Antarctic fossil penguin collection and Carl Wiman's contribution. *Polar Record*, 53:364-375. <https://doi.org/10.1017/S0032247417000249>
- Acosta Hospitaleche, C. and Jadwiszczak, P. 2011. Enigmatic morphological disparity in tarsometatarsi of giant penguins from the Eocene of Antarctica. *Polish Polar Research*, 32:175-180. <https://doi.org/10.2478/v10183-011-0013-9>
- Acosta Hospitaleche, C. and Olivero, E. 2016. Re-evaluation of the fossil penguin *Palaeudyptes gunnari* from the Eocene Leticia Formation, Argentina: Additional material, systematics and palaeobiology. *Alcheringa*, 40:373-382. <https://doi.org/10.1080/03115518.2016.1144994>
- Acosta Hospitaleche, C. and Reguero, M. 2010. First articulated skeleton of *Palaeudyptes gunnari* from the late Eocene of Isla Marambio (Seymour Island), Antarctica. *Antarctic Science*, 22:289-298. <https://doi.org/10.1017/S0954102009990769>
- Acosta Hospitaleche, C. and Reguero, M. 2014. *Palaeudyptes klekowskii*, the best preserved penguin skeleton from the Eocene-Oligocene of Antarctica: Taxonomic and evolutionary remarks. *Geobios*, 47:77-85. <https://doi.org/10.1016/j.geobios.2014.03.003>
- Acosta Hospitaleche, C., Reguero, M., and Santillana, S. 2017b. *Aprosdokitos mikrotero* gen. et sp. nov., the tiniest Sphenisciformes that lived in Antarctica during the Paleogene. *Neues Jahrbuch für Geologie und Paläontologie – Abhandlungen*, 283:25-34. <https://doi.org/10.1127/njgpa/2017/0624>
- Acosta Hospitaleche, C., Tambussi, C., Donato, M., and Cozzuol, M. 2007. A new Miocene penguin from Patagonia and its phylogenetic relationships. *Acta Palaeontologica Polonica*, 52:299-314.
- Alara Team, 2005-2013. CRystalView veterinary software. Alara Inc., Fremont, CA, USA. <http://www.alara.com> (no longer active)
- Andersson, G.L. 1906. On the geology of Graham Land. *University of Uppsala Geological Institute Bulletin*, 7:19-71.
- Bargo, M.S. and Reguero, M.A. 1998. Annotated catalogue of the fossil vertebrates from Antarctica housed in the Museo de La Plata, Argentina. I. Birds and land mammals from La

- Meseta Formation (Eocene-?early Oligocene), p. 211-221. In Casadio, S. (ed.), *Paleógeno de América del Sur y de la Península Antártica (Volume 5)*. Asociación Paleontológica Argentina Publicación Especial, Buenos Aires.
- Baumel, J.J. and Raikow, R.J. 1993. Arthrologia, p. 133-187. In Baumel, J.J. (ed.), *Handbook of Avian Anatomy: Nomina Anatomica Avium*. Nutall Ornithological Club, Cambridge, Massachusetts.
- Baumel, J.J. and Witmer, L.M. 1993. Osteologia, p. 45-132. In Baumel, J.J. (ed.), *Handbook of Avian Anatomy: Nomina Anatomica Avium*. Nutall Ornithological Club, Cambridge, Massachusetts.
- Bertelli, S., Giannini, N.P., and Ksepka, D.T. 2006. Redescription and phylogenetic position of the Early Miocene Penguin *Paraptenodytes antarcticus* from Patagonia. *American Museum Novitates*, 3525:1-36. [https://doi.org/10.1206/0003-0082\(2006\)3525%5B1:RAPPO%5D2.0.CO;2](https://doi.org/10.1206/0003-0082(2006)3525%5B1:RAPPO%5D2.0.CO;2)
- Bonaparte, C.L. 1831. Saggio di una distribuzione metodica degli animali vertebrati. *Giornale Arcadico di Scienze Lettere ed Arti*, 52:155-189.
- Bonhomme, V., Picq, S., Gaucherel, C., and Claude, J. 2014. Momocs: Outline analysis using R. *Journal of Statistical Software*, 56(13). <https://doi.org/10.18637/jss.v056.i13>
- Brassey, C. 2016. Body-mass estimation in paleontology: A review of volumetric techniques. *The Paleontological Society Papers*, 22:133-156. <https://doi.org/10.1017/scs.2017.12>
- Buono, M.R., Fernández, M.S., Reguero, M.A., Marenssi, S.A., Santillana, S.N., and Mörs, T. 2016. Eocene basilosaurid whales from the La Meseta Formation, Marambio (Seymour) Island, Antarctica. *Ameghiniana*, 53:296-315. <https://doi.org/10.5710/AMGH.02.02.2016.2922>
- Clarke, J.A., Ksepka, D.T., Salas-Gismondi, R., Altamirano, A.J., Shawkey, M.D., D'Alba, L., Vinther, J., DeVries, T.J., Baby, P. 2010. Fossil evidence for evolution of the shape and color of penguin feathers. *Science*, 330:954-957. <https://doi.org/10.1126/science.1193604>
- Clarke, J.A., Ksepka, D.T., Stucchi, M., Urbina, M., Giannini, N., Bertelli, S., Narváez, Y., and Boyd, C.A. 2007. Paleogene equatorial penguins challenge the proposed relationship between biogeography, diversity, and Cenozoic climate change. *Proceedings of the National Academy of Sciences*, 104:11545-11550. <https://doi.org/10.1073/pnas.0611099104>
- Clarke, J.A., Olivero, E.B., and Puerta, P. 2003. Description of the earliest fossil penguin from South America and first Paleogene vertebrate locality of Tierra del Fuego, Argentina. *American Museum Novitates*, 423:1-18. [https://doi.org/10.1206/0003-0082\(2003\)423<0001:DOTEFP>2.0.CO;2](https://doi.org/10.1206/0003-0082(2003)423<0001:DOTEFP>2.0.CO;2)
- Cornthwaite, J. 2013. Species natural history, p. 190-237. In De Roy, T., Jones, M., and Cornthwaite, J. (eds.), *Penguins. The Ultimate Guide*. Princeton University Press, Princeton, New Jersey.
- Dann, P., Carron, M., Chambers, B., Chambers, L., Dornom, T., McLaughlin, A., Sharp, B., Talmage, M.E., Thoday, R., and Unthank, S. 2005. Longevity in little penguins *Eudyptula minor*. *Marine Ornithology*, 33:71-72.
- Del Hoyo, J., Elliott, A., and Sargatal, J. 1992. *Handbook of the Birds of the World. Volume I. Ostrich to Ducks*. Lynx Edicions, Barcelona.
- Douglas, P.M., Affek, H.P., Ivany, L.C., Houben, A.J., Sijp, W.P., Sluijs, A., Schouten, S., and Pagani, M. 2014. Pronounced zonal heterogeneity in Eocene southern high-latitude sea surface temperatures. *Proceedings of the National Academy of Sciences of the United States of America*, 111:6582-6587. <https://doi.org/10.1073/pnas.1321441111>
- Forster, J.R. 1781. Historia Aptenodytae. *Commentationes Societatis Regiae Scientiarum Gottingensis*, 3:121-148.
- Gavryushkina, S., Heath, T.A., Ksepka, D.T., Stadler, T., Welch, D., and Drummond, A.J. 2017. Bayesian total-evidence dating reveals the recent crown radiation of penguins. *Systematic Biology*, 66:57-73. <https://doi.org/10.1093/sysbio/syw060>
- Gray, G.R. 1844. On *Aptenodytes*. *Annals and Magazine of Natural History*, 13:315.
- Hackett, S.J., Kimball, R.T., Reddy, S., Bowie, R.C.K., Braun, E.L., Braun, M.J., Chojnowski, J.L., Cox, W.A., Han, K.-L., Harshman, J., Huddleston, C.J., Marks, B.D., Miglia, K.J., Moore, W.S., Sheldon, F.H., Steadman, D.W., Witt, C.C., and Yuri, T. 2008. Phylogenomic study of birds reveals their evolutionary history. *Science*, 320:1763-1768. <https://doi.org/10.1126/science.1157704>

- Hutchinson, J.R. 2001. The evolution of pelvic osteology and soft tissues on the line to extant birds (Neornithes). *Zoological Journal of the Linnean Society*, 131:123-168. <https://doi.org/10.1006/zjls.2000.0254>
- Huxley, T.H. 1859. On a fossil bird and a fossil cetacean from New Zealand. *Quarterly Journal of the Geological Society of London*, 15:670-677.
- Ibáñez, B and Tambussi, C.P. 2012. Foot-propelled aquatic birds: pelvic morphology and locomotor performance. *Italian Journal of Zoology*, 79:356-362. <https://doi.org/10.1080/11250003.2011.650713>
- Jadwiszczak, P. 2001. Body size of Eocene Antarctic penguins. *Polish Polar Research*, 22:147-158.
- Jadwiszczak, P. 2006. Eocene penguins of Seymour Island, Antarctica: Taxonomy. *Polish Polar Research*, 27:3-62.
- Jadwiszczak, P. 2008. An intriguing penguin bone from the Late Eocene of Seymour Island (Antarctic Peninsula). *Antarctic Science*, 20:589-590. <https://doi.org/10.1017/S0954102008001405>
- Jadwiszczak, P. 2009. Penguin past: The current state of knowledge. *Polish Polar Research*, 30:3-28.
- Jadwiszczak, P. 2010. New data on the appendicular skeleton and diversity of Eocene Antarctic penguins, p. 44-50. In Nowakowski, D. (ed.), *Morphology and Systematics of Fossil Vertebrates*. DN Publishers, Wrocław, Poland.
- Jadwiszczak, P. 2011. New data on morphology of late Eocene penguins and implications for their geographic distribution. *Antarctic Science*, 23:605-606. <https://doi.org/10.1017/S0954102011000526>
- Jadwiszczak, P. 2012. Partial limb skeleton of a "giant penguin" *Anthropornis* from the Eocene of Antarctic Peninsula. *Polish Polar Research*, 33:259-274. <https://doi.org/10.2478/v10183-012-0017-0>
- Jadwiszczak, P. 2013. Taxonomic diversity of Eocene Antarctic penguins: A changing picture, p. 129-138. In Hambrey, M.J., Barker, P.F., Barrett, P.J., Bowman, V., Davies, B., Smellie, J.L., and Tranter, M. (eds.), *Antarctic Palaeoenvironments and Earth-Surface Processes. Geological Society Special Publications*, 381. <https://doi.org/10.1144/SP381.7>
- Jadwiszczak, P. 2014. Synsacra of the Eocene Antarctic penguins: New data on spinal maturation and an insight into their role in the control of walking. *Polish Polar Research*, 35:27-39. <https://doi.org/10.2478/popore-2014-0005>
- Jadwiszczak, P. 2015. Another look at tarsometatarsi of early penguins. *Polish Polar Research*, 36:343-354. <https://doi.org/10.1515/popore-2015-0024>
- Jadwiszczak, P., Acosta Hospitaleche, C., and Reguero, M. 2013. Redescription of *Crossvallia unienwillia* - the only Paleocene Antarctic penguin. *Ameghiniana*, 50:545-553. <https://doi.org/10.5710/AMGH.09.10.2013.1058>
- Jadwiszczak, P. and Chapman, S.D. 2011. The earliest fossil record of a medium-sized penguin. *Polish Polar Research*, 32:269-277. <https://doi.org/10.2478/v10183-011-0020-x>
- Jadwiszczak, P. and Mörs, T. 2011. Aspects of diversity in early Antarctic penguins. *Acta Palaeontologica Polonica*, 56:269-277. <https://doi.org/10.4202/app.2009.1107>
- Jadwiszczak, P. and Mörs, T. 2017. An enigmatic fossil penguin from the Eocene of Antarctica. *Polar Research*, 36:1291086. <https://doi.org/10.1080/17518369.2017.1291086>
- Jarvis, E.D., Mirarab, S., Aberer, A.J., Li, B., Houde, P., Li, C., Ho, S.Y., Faircloth, B.C., Nabholz, B., Howard, J.T., Suh, A., Weber, C.C., da Fonseca, R.R., Li, J., Zhang, F., Li, H., Zhou, L., Narula, N., Liu, L., Ganapathy, G., Boussau, B., Bayzid, M.S., Zavidovych, V., Subramanian, S., Gabaldón, T., Capella-Gutiérrez, S., Huerta-Cepas, J., Rekepalli, B., Munch, K., Schierup, M., Lindow, B., Warren, W.C., Ray, D., Green, R.E., Bruford, M.W., Zhan, X., Dixon, A., Li, S., Li, N., Huang, Y., Derryberry, E.P., Bertelsen, M.F., Sheldon, F.H., Brumfield, R.T., Mello, C.V., Lovell, P.V., Wirthlin, M., Schneider, M.P., Prosdocimi, F., Samaniego, J.A., Vargas Velazquez, A.M., Alfaro-Núñez, A., Campos, P.F., Petersen, B., Sicheritz-Ponten, T., Pas, A., Bailey, T., Scofield, P., Bunce, M., Lambert, D.M., Zhou, Q., Perelman, P., Driskell, A.C., Shapiro, B., Xiong, Z., Zeng, Y., Liu, S., Li, Z., Liu, B., Wu, K., Xiao, J., Yinqi, X., Zheng, Q., Zhang, Y., Yang, H., Wang, J., Smeds, L., Rheindt, F.E., Braun, M., Fjeldsa, J., Orlando, L., Barker, F.K., Jönsson, K.A., Johnson, W., Koepfli, K.P., O'Brien, S., Haussler, D., Ryder, O.A., Rahbek, C., Willerslev, E., Graves, G.R., Glenn, T.C., McCormack, J., Burt, D., Ellegren, H., Alström, P., Edwards, S.V., Stamatakis, A., Mindell, D.P., Cracraft, J., Braun, E.L., Warnow, T., Jun, W., Gilbert, M.T. and Zhang, G. 2014. Whole-genome analyses resolve

- early branches in the tree of life of modern birds. *Science*, 346:1320-1331. <https://doi.org/10.1126/science.1253451>
- Klemm, R.D. 1969. *Comparative Myology of the Hind Limb of Procellariiform Birds*. Southern Illinois University Monographs, Science Series, No. 2, Carbondale, Illinois.
- Kriwet, J., Engelbrecht, A., Mörs, T., Reguero, M., and Pfaff, C. 2016. Ultimate Eocene (Priabonian) chondrichthyans (Holocephali, Elasmobranchii) of Antarctica. *Journal of Vertebrate Paleontology*, 30:e1160911. <https://doi.org/10.1080/02724634.2016.1160911>
- Ksepka, D.T. and Ando, T. 2011. Penguins past, present, and future: Trends in the evolution of the Sphenisciformes, p. 155-186. In Dyke, G. and Kaiser, G. (eds.), *Living Dinosaurs: The Evolutionary History of Modern Birds*. John Wiley and Sons, Chichester.
- Ksepka, D.T. and Clarke, J.A. 2010. The basal penguin (Aves, Sphenisciformes) *Perudyptes devriesi* and a phylogenetic evaluation of the penguin fossil record. *Bulletin of the American Museum of Natural History*, 337:1-77. <https://doi.org/10.1206/653.1>
- Ksepka, D.T., Fordyce, R.E., Ando, T., and Jones, C.M. 2012. New fossil penguins (Aves, Sphenisciformes) from the Oligocene of New Zealand reveal the skeletal plan of stem penguins. *Journal of Vertebrate Palaeontology*, 32:235-254. <https://doi.org/10.1080/02724634.2012.652051>
- Kuznetsov, A.N. and Sennikov, A.G. 2000. On the function of a perforated acetabulum in archosaurs and birds. *Paleontological Journal*, 34:439-448.
- Linnaeus, C. 1758. *Systema Naturae per Regna Tria Naturae, Secundum Classes, Ordines, Genera, Species, cum Characteribus, Differentiis, Synonymis, Locis (Ed 10, Tomus 1)*. Laurentii Salvii, Stockholm.
- Marenssi, S.A. 2006. Eustatically controlled sedimentation recorded by Eocene strata of the James Ross Basin, Antarctica. *Geological Society London, Special Publications*, 258:125-133. <https://doi.org/10.1144/GSL.SP.2006.258.01.09>
- Marples, B.J. 1952. Early Tertiary penguins of New Zealand. *New Zealand Geological Survey Paleontological Bulletin*, 20:1-66.
- Mayr, G. 2009. Notes on the osteology and phylogenetic affinities of the Oligocene Diomedoididae (Aves, Procellariiformes). *Fossil Record*, 12:133-140. <https://doi.org/10.5194/fr-12-133-2009>
- Mayr, G., De Pietri, V.L., Love, L., Mannering, A.A., and Scofield, R.P. 2018. A well-preserved new mid-Paleocene penguin (Aves, Sphenisciformes) from the Waipara Greensand in New Zealand. *Journal of Vertebrate Paleontology*, 37:6. <https://doi.org/10.1080/02724634.2017.1398169>
- Mayr, G., De Pietri, V.L., and Scofield, R.P. 2017a. A new fossil from the mid-Paleocene of New Zealand reveals an unexpected diversity of world's oldest penguins. *Science of Nature*, 104:9. <https://doi.org/10.1007/s00114-017-1441-0>
- Mayr, G. and Goedert, J.L. 2018. First record of a tarsometatarsus of *Tonsala hildegardae* (Plotopteridae) and other avian remains from the late Eocene/early Oligocene of Washington State (USA). *Geobios*, 51:51-59. <https://doi.org/10.1016/j.geobios.2017.12.006>
- Mayr, G., Scofield, R.P., De Pietri, V.L., and Tennyson, A.J.D. 2017b. A Paleocene penguin from New Zealand substantiates multiple origins of gigantism in fossil Sphenisciformes. *Nature Communications*, 8:1927. <https://doi.org/10.1038/s41467-017-01959-6>
- Meyen, F.J.F. 1834. Vögel. *Nova Acta Physico-Medica Academiae Caesareae Leopoldino-Carolinae Naturae Curiosorum*, 16:59-124.
- Midtgård, U. 1982. Patterns in the blood vascular system in the pelvic limb of birds. *Journal of Zoology*, 196:545-567. <https://doi.org/10.1111/j.1469-7998.1982.tb03523.x>
- Miller, J.F. 1778. *Icones Animalium et Plantarum (Pt. 4)*. Published privately, London.
- Montes, M., Nozal, F., Santillana, S., Marenssi, S., and Olivero, E. 2013. *Mapa Geológico de la Isla Marambio (Seymour); escala 1:20.000. Serie Cartográfica Geocientífica Antártica. Con texto complementario*. Instituto Geológico y Minero de España, Madrid and Instituto Antártico Argentino, Buenos Aires.
- Moreno, F.P. and Mercerat A. 1891. Catalogo de los pájaros fósiles de la República Argentina conservados en el Museo de La Plata. *Anales del Museo de La Plata. Paleontología Argentina*, 1:7-71.
- Myrcha, A., Jadwiszczak, P., Tambussi, C.P., Noriega, J.I., Gaździcki, A., Tatur, A., and Del Valle, R.A. 2002. Taxonomic revision of Eocene Antarctic penguins based on tarsometatarsal morphology. *Polish Polar Research*, 23:5-46.

- Myrcha, A., Tatur, A., and Del Valle, R. 1990. A new species of fossil penguin from Seymour Island, West Antarctica. *Alcheringa*, 14:195-205.
- Necker, R. 2006. Specializations in the lumbosacral vertebral canal and spinal cord of birds: Evidence of a function as a sense organ which is involved in the control of walking. *Journal of Comparative Physiology A*, 192:439-448. <https://doi.org/10.1007/s00359-006-0105-x>
- Park, T. and Fitzgerald, E.M.G. 2012. A review of Australian fossil penguins (Aves: Sphenisciformes). *Memoirs of Museum Victoria*, 69:309-325. <https://doi.org/10.24199/j.mmv.2012.69.06>
- Perumal, V., Woodley, S.J., and Nicholson, H.D. 2017. The morphology and morphometry of the fovea capititis femoris. *Surgical and Radiologic Anatomy*, 39:791-798. <https://doi.org/10.1007/s00276-016-1810-y>
- R Core Team 2017. *R: A language and environment for statistical computing*. The R Foundation for Statistical Computing, Vienna. <http://www.r-project.org>
- Sadler, P.M. 1988. Geometry and stratification of uppermost Cretaceous and Paleogene units on Seymour Island, northern Antarctic Peninsula, p. 303-320. In Feldmann, R.M. and Woodburne, M.O. (eds.), *Geology and Paleontology of Seymour Island, Antarctic Peninsula*. Geological Society of America Memoirs, 169, Boulder, Colorado.
- Santesoft Team 2018. Sante DICOM Viewer Free 5.4.3. Santesoft LTD, Nicosia, Cyprus. <https://www.santesoft.com>
- Schindelin, J., Arganda-Carreras, I., Frise, E., Kaynig, V., Longair, M., Pietzsch, T., Preibisch, S., Rueden, C., Saalfeld, S., Schmid, B., Tinevez, J.Y., White, D.J., Hartenstein, V., Eliceiri, K., Tomancak, P., and Cardona, A. 2012. Fiji: an opensource platform for biological-image analysis. *Nature Methods*, 9:676-682. <https://doi.org/10.1038/nmeth.2019>
- Schreiber, E.A. and Burger, J. 2002. Seabirds in the marine environment, p. 1-15. In Schreiber, E.A. and Burger, J. (ed.), *Biology of Marine Birds*. CRC Press, Boca Raton.
- Schreiweis, D.O. 1982. A comparative study of the appendicular musculature of penguins (Aves: Sphenisciformes). *Smithsonian Contributions to Zoology*, 341:1-46.
- Sharpe, R.B. 1891. *A Review of Recent Attempts to Classify Birds*. Hungarian Committee of II International Ornithological Congress, Budapest.
- Simpson, G.G. 1946. Fossil penguins. *Bulletin of the American Museum of Natural History*, 87:1-99.
- Simpson, G.G. 1971. Review of fossil penguins from Seymour Island. *Proceedings of the Royal Society of London B*, 178:357-387.
- Simpson, G.G. 1976. *Penguins: Past and Present, Here and There*. Yale University Press, New Haven and London.
- Slack, K.E., Jones, C.M., Ando, T., Harrison, G.L., Fordyce, R.E., Arnason, U., and Penny, D. 2006. Early penguin fossils, plus mitochondrial genomes, calibrate avian evolution. *Molecular Biology and Evolution*, 23:1144-1155. <https://doi.org/10.1093/molbev/msj124>
- Stephan, B. 1979. Vergleichende Osteologie der Pinguine. *Mitteilungen aus dem Zoologischen Museum in Berlin*, 55(3, Supplement):3-98.
- Subramanian, S., Beans-Picón, G., Swaminathan, S.K., Millar, C.D., and Lambert, D.M. 2013. Evidence for a recent origin of penguins. *Biology Letters*, 9:20130748. <https://doi.org/10.1098/rsbl.2013.0748>
- Tambussi, C.P., Reguero, M.A., Marenssi, S.A., and Santillana, S.N. 2005. *Crossvallia unienwillia*, a new Spheniscidae (Sphenisciformes, Aves) from the late Paleocene of Antarctica. *Geobios*, 38:667-675. <https://doi.org/10.1016/j.geobios.2004.02.003>
- Wickham, H. 2009. *ggplot2: Elegant Graphics for Data Analysis*. Springer-Verlag, New York, New York.
- Wideman, R.F., Jr. 2016. Bacterial chondronecrosis with osteomyelitis and lameness in broilers: A review. *Poultry Science*, 95:325-344. <https://doi.org/10.3382/ps/pev320>
- Wilcox, H.H. 1952. The pelvic musculature of the loon, *Gavia immer*. *The American Midland Naturalist*, 48:513-573. <https://doi.org/10.2307/2422198>
- Williams, T.D. 1995. *The Penguins*. Oxford University Press, New York, New York.
- Wiman, C. 1905. Über die alttertiären Vertebraten der Seymourinsel. In Nordenskjöld, O. (ed.), *Wissenschaftliche Ergebnisse der Schwedischen Südpolar-Expedition 1901-1903, Band III, Lieferung I*. Lithographisches Institut des Generalstabs, Stockholm.
- Zeffner, A. and Norberg, U.M.L. 2003. Leg morphology and locomotion in birds: requirements for force and speed during ankle flexion. *Journal of Experimental Biology*, 206:1085-1097. <https://doi.org/10.1242/jeb.00208>

Zusi, R.L. 1975. An interpretation of skull structure in penguins, p. 59-84. In Stonehouse, B. (ed.), *The Biology of Penguins*. The Macmillan Press Ltd., London and Basingstoke.

APPENDIX 1.

Comparative material utilized in Figures 3 and 6. Other specimens used for comparisons are referenced in-text, either via their catalog numbers (if they were studied directly) or by citations of source works with relevant figure/table numbers.

1. Tarsometatarsi used in Figure 3. Data for fossil specimens from IB/P/B and MLP after Myrcha et al. (2002, table 1), CM - after Slack et al. (2006) and Mayr et al. (2017a), MUSM – after Clarke et al. (2010), OU - after Marples (1952) and Ksepka et al. (2012); Trochlear widths for *Inkayacu*, *Kairuku*, *Muriwaimanu*, *Waimanu*, and CM 2016.158.1 as well as midwidths of *Muriwaimanu*, *Waimanu* and CM 2016.158.1 were assessed based on published photographs (with scales). Other measurements were taken directly by PJ.

a. Fossil bones

- Anthropornis grandis*
IB/P/B-0483, MLP 95-I-10-142, MLP 94-III-15-178
- Anthropornis nordenskjoeldi*
NRM-PZ A.45
- Archaeospheniscus lopdelli*
NHMUK A4080 (cast)
- Archaeospheniscus wimani*
MLP 90-I-20-24, NHMUK A3331
- Delphinornis arctowskii*
IB/P/B-0484, MLP 93.X.1.92
- Delphinornis gracilis*
IB/P/B-0279a
- Delphinornis larseni*
NRM-PZ A.21, NRM-PZ A.587, NRM-PZ A.861, NRM-PZ A.895, IB/P/B-0062, IB/P/B-0547, IB/P/B-0548, MLP 84.II.1.79, MLP 91.II.4.174, MLP 83.V.20.5
- Inkayacu paracasensis*
MUSM 1444
- Kairuku grebneffi*
OU 22094
- Kairuku waitaki*
OU 12652
- Korora oliveri*
OU C.50.63
- Marambiornis exilis*
IB/P/B-0490, MLP 93.X.1.111
- Mesetaornis polaris*
IB/P/B-0278
- Muriwaimanu tuatahi*
CM zfa 34
- Palaeudyptes antarcticus*
NHMUK A1048
- Palaeudyptes gunnari*
IB/P/B-0072, IB/P/B-0277, IB/P/B-0487, MLP 91-II-4-222, MLP 87-II-1-45, MLP 82-IV-23-6, MLP 84-II-1-124'
- Palaeudyptes klekowskii*
IB/P/B-0485, IB/P/B-0545, IB/P/B-0546, MLP 93-X-1-142, MLP 84-II-1-78, MLP 93-X-1-63, MLP 84-II-1-76, MLP 93-X-1-106, MLP 94-III-15-20, MLP 83-V-30-15, MLP 83-V-30-16, MLP 84-II-1-124
- Palaeudyptes marplesi*
NHMUK A6119 (cast)
- Waimanu manneringi*
CM zfa 35

Undetermined Paleocene penguin from New Zealand
CM 2016.158.1

b. Modern bones

Aptenodytes forsteri

NHMUK/T 1197A, NHMUK/T 1197D, NHMUK/T 1197B, NHMUK/T 1972.1.25, NHMUK/T 1905.12.30.419, NHMUK/T 1998.55.2

Aptenodytes patagonicus

NHMUK/T 1846.4.15.33, NHMUK/T 701A, NHMUK/T 701B, NHMUK/T 1952.1.28, NHMUK/T 1972.1.24, NHMUK/T 2000.12.1

Eudyptes chrysocome

NHMUK/T 1952.1.39, NHMUK/T 1898.7.1.15, NHMUK/T 1964.14.2, NHMUK/T 1898.7.1.14

Eudyptula minor

NHMUK/T 1966.51.1, NHMUK/T 2002.2.1, NHMUK/T 1896.2.16.38

Pygoscelis adeliae

NHMUK/T 1849.10.2.2, NHMUK/T 1850.9.7.1, IB/P/B – three unnumbered specimens.

Pygoscelis papua

NHMUK/T 2006.1.16, IB/P/B - an unnumbered specimen,

Spheniscus demersus

NHMUK/T 1898.7.1.8, NHMUK/T 1898.7.1.9, NHMUK/T 1998.23.2, NHMUK/T 1998.48.24

2. Hip bones specimens used in Figure 6. Outlines of foramina for *Kairuku grebneffi* and *Waimanu manneringi* were assessed based on Ksepka et al. (2012, figure 6) and Slack et al. (2006, figure 1) respectively.

a. Fossil

Kairuku grebneffi

OU 22094

Waimanu manneringi

CM zfa 35

b. Modern

Aptenodytes forsteri

NHMUK/T 1972.1.25

Aptenodytes patagonicus

NHMUK/T 1846.4.15.32

Eudyptes chrysocome

NHMUK/T 1956.14.1

Eudyptula minor

NHMUK/T 2002.2.1

Pygoscelis adeliae

IB/P/B - an unnumbered specimen

Pygoscelis papua

IB/P/B - an unnumbered specimen

Spheniscus demersus

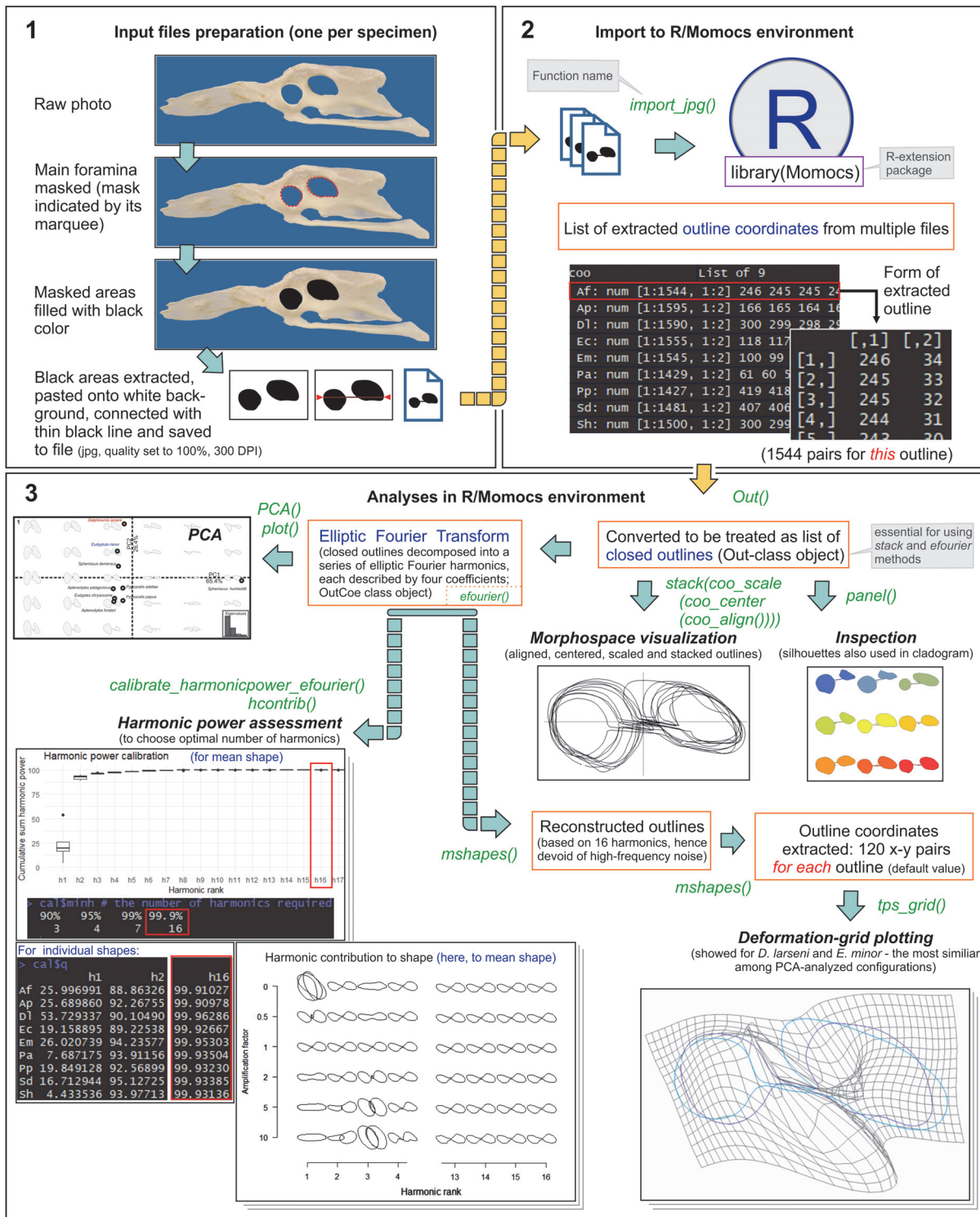
NHMUK/T 1905.5.23.1

Spheniscus humboldti

NHMUK/T 1952.1.42

APPENDIX 2.

Details of the shape-analysis workflow.



APPENDIX 3.

Harmonic coefficients (normalized) calculated for outlines of major hip bone foramina (nine outlines \times 16 harmonics, four coefficients for each harmonic).

Jadwiszczak and Mörs, First partial skeleton of *Delphinornis larseni* Wiman, 1905, a slender-footed penguin from the Eocene of Antarctic Peninsula.

APPENDIX 3. Harmonic coefficients (normalized) calculated for outlines of major hip bone foramina (nine outlines \times 16 harmonics, four coefficients for each harmonic).

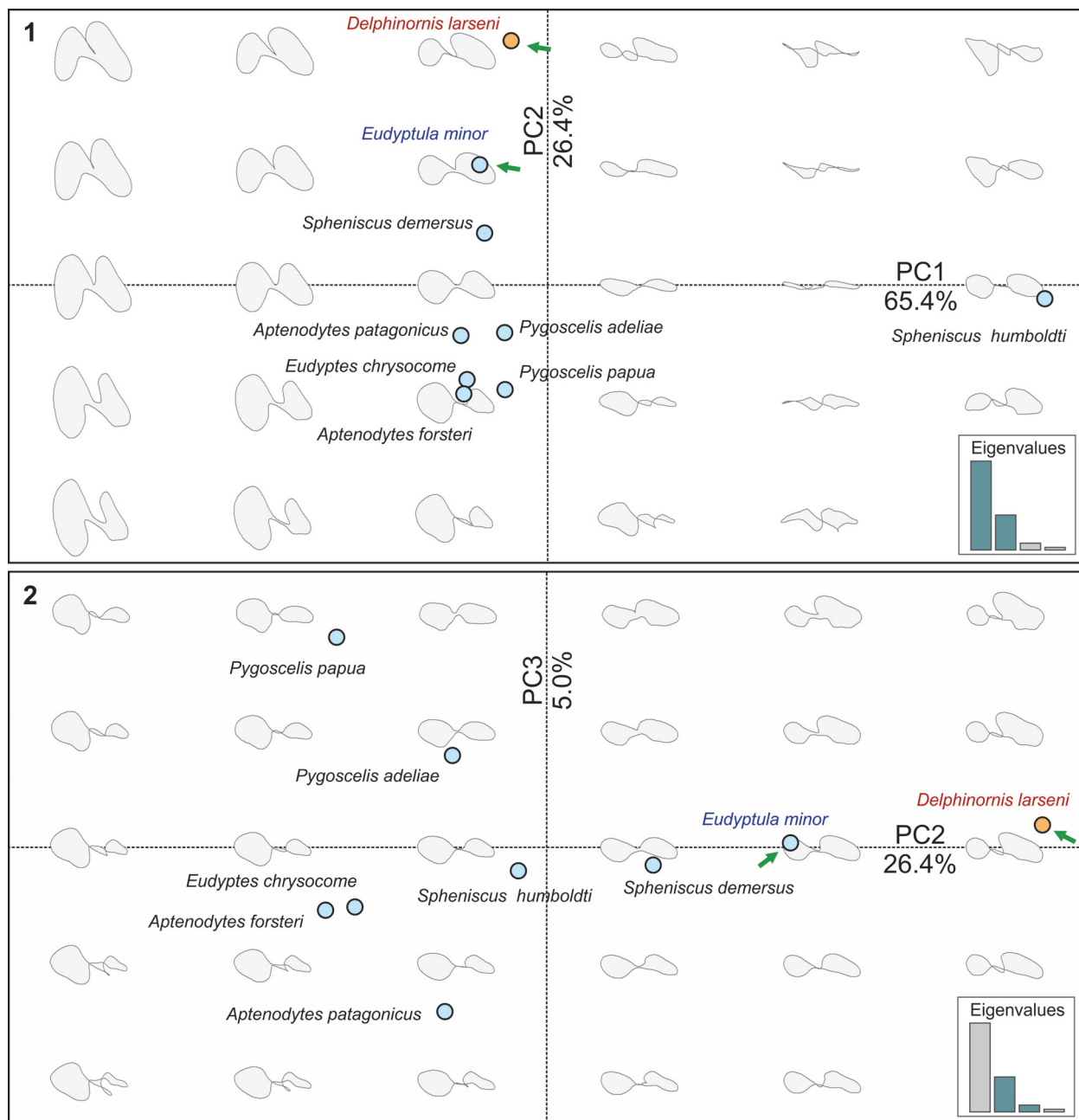
	A1	A2	A3	A4	A5	A6	A7
<i>A. forsteri</i>	1.000000	0.035786	0.133590	-0.002903	0.017254	-0.018801	-0.010171
<i>A. patagonicus</i>	1.000000	0.067544	0.158027	-0.019771	0.024652	0.003973	-0.022821
<i>D. larseni</i>	1.000000	-0.076995	0.174987	0.012179	-0.032708	-0.012419	0.009728
<i>E. chrysocome</i>	1.000000	0.038634	0.138061	-0.003595	0.028278	-0.023276	-0.009829
<i>E. minor</i>	1.000000	-0.008912	0.155486	0.004365	-0.004620	0.025240	0.002692
<i>P. adeliae</i>	1.000000	-0.023009	0.160485	-0.001064	0.019697	-0.010874	-0.004514
<i>P. papua</i>	1.000000	-0.017745	0.165500	-0.017904	0.006324	-0.009807	0.012399
<i>S. demerus</i>	1.000000	-0.008206	0.150995	-0.003024	0.023549	0.019210	-0.012416
<i>S. humboldti</i>	1.000000	-0.016275	0.151114	-0.003572	0.025483	0.014327	-0.010148
	B1	B2	B3	B4	B5	B6	B7
<i>A. forsteri</i>	0.000000	-0.066369	0.077434	-0.046354	0.017405	0.010943	-0.002811
<i>A. patagonicus</i>	0.000000	-0.138297	0.099830	-0.060066	-0.007940	0.021092	0.033620
<i>D. larseni</i>	0.000000	-0.294488	-0.028716	-0.000089	0.005157	-0.068034	-0.014133
<i>E. chrysocome</i>	0.000000	-0.053677	0.073756	-0.049932	0.012276	0.021648	0.007629
<i>E. minor</i>	0.000000	-0.166471	0.027444	0.000916	-0.020699	-0.026779	0.022776
<i>P. adeliae</i>	0.000000	-0.024607	0.032631	-0.007803	-0.002715	0.001851	0.016961
<i>P. papua</i>	0.000000	0.056545	0.007133	0.003373	0.002915	0.005710	0.004768
<i>S. demerus</i>	0.000000	-0.130001	0.045129	-0.018012	-0.015749	-0.011905	0.035785
<i>S. humboldti</i>	0.000000	0.058072	-0.039889	-0.003574	0.012208	0.018226	-0.026498
	C1	C2	C3	C4	C5	C6	C7
<i>A. forsteri</i>	0.000000	-0.046828	-0.016487	0.008143	-0.007220	0.020121	0.000854
<i>A. patagonicus</i>	0.000000	-0.069232	-0.059733	0.007309	-0.002458	0.006201	0.008297
<i>D. larseni</i>	0.000000	-0.041711	-0.144774	-0.097485	0.001300	-0.027899	0.005981
<i>E. chrysocome</i>	0.000000	-0.062813	-0.031994	0.010307	-0.001180	0.014191	0.004156
<i>E. minor</i>	0.000000	-0.068977	-0.095783	-0.025213	0.006385	-0.013783	0.017435
<i>P. adeliae</i>	0.000000	-0.021207	-0.050750	0.017365	0.009700	0.001596	0.006169
<i>P. papua</i>	0.000000	0.025050	-0.053472	0.021913	0.012772	0.006802	-0.001025
<i>S. demerus</i>	0.000000	-0.066140	-0.081206	-0.007872	0.008306	-0.005627	0.017985
<i>S. humboldti</i>	0.000000	0.002107	-0.051842	-0.007601	0.006532	-0.004929	0.011913
	D1	D2	D3	D4	D5	D6	D7
<i>A. forsteri</i>	-0.347374	-0.170325	-0.255344	0.095882	0.009473	-0.010230	-0.004098
<i>A. patagonicus</i>	-0.312126	-0.121268	-0.270959	0.045558	0.025827	-0.017454	0.004731
<i>D. larseni</i>	-0.304816	0.163042	-0.171745	-0.062039	-0.007063	0.016434	-0.003140
<i>E. chrysocome</i>	-0.335861	-0.133744	-0.264986	0.082370	0.023491	-0.018382	0.002992
<i>E. minor</i>	-0.309237	0.080586	-0.257265	-0.054735	0.012556	0.023382	-0.008356
<i>P. adeliae</i>	-0.313182	-0.076122	-0.231917	0.031058	0.040847	-0.008925	-0.030261
<i>P. papua</i>	-0.360038	-0.126847	-0.207726	0.053627	0.038066	-0.023022	-0.020622
<i>S. demerus</i>	-0.296603	0.008250	-0.262423	-0.022735	0.032945	0.007891	-0.007402
<i>S. humboldti</i>	0.277739	-0.028478	0.250630	0.040632	-0.022270	-0.014213	0.012320

APPENDIX 3 (CONTINUED).

A8	A9	A10	A11	A12	A13	A14	A15	A16
0.027162	-0.013970	-0.007871	0.000852	0.002533	-0.009810	0.004728	0.001243	-0.001822
0.012959	0.008636	-0.006695	-0.005926	0.006857	-0.000997	-0.005413	0.000872	0.001985
0.018772	0.001718	0.001622	-0.005688	-0.001997	-0.000919	0.001161	-0.001244	-0.000978
0.025482	-0.004261	-0.005220	0.004147	0.001417	-0.005659	0.000398	0.000081	0.000598
-0.006178	-0.006856	0.006280	0.003676	0.001049	-0.000059	-0.000402	0.002507	-0.001801
0.005696	0.012438	-0.007647	-0.007089	0.003314	0.002768	-0.003118	-0.001520	0.002835
-0.002751	0.004091	-0.006405	0.004221	-0.002170	0.000413	-0.001931	0.003361	0.000070
-0.009333	0.007907	0.011004	-0.004319	-0.001984	0.000073	0.003815	-0.002434	-0.002506
-0.017709	0.006951	0.008081	-0.006046	-0.005728	0.000040	0.001070	-0.001616	-0.001211
B8	B9	B10	B11	B12	B13	B14	B15	B16
-0.018763	0.015603	-0.003158	-0.004909	0.002695	0.001318	0.001283	0.003309	-0.001630
-0.032812	0.005399	0.013294	-0.002141	-0.000020	0.001276	0.001373	-0.001894	0.002875
0.010811	0.014850	0.003575	-0.001014	-0.004365	-0.001045	0.004444	0.000404	-0.004292
-0.019109	0.014112	-0.000065	-0.000862	-0.002091	-0.001518	-0.000356	0.000557	-0.001122
0.020568	-0.003704	-0.008676	-0.001494	0.008097	-0.000214	-0.001406	-0.002045	0.002143
-0.013088	-0.001741	0.003595	0.003090	-0.006604	0.001524	0.003434	-0.000157	-0.003918
-0.008252	-0.001638	0.003728	-0.001322	-0.006307	0.002722	0.004228	-0.004580	-0.001935
-0.001990	-0.011731	-0.005512	0.008245	0.001866	-0.003963	-0.000144	0.000332	-0.000858
-0.005246	0.007524	0.006890	-0.006692	-0.000753	-0.000193	-0.001932	-0.000648	0.002764
C8	C9	C10	C11	C12	C13	C14	C15	C16
-0.004366	0.008512	-0.007555	-0.006546	-0.005315	0.009467	-0.001163	-0.004002	0.006001
-0.024647	0.013394	0.003694	0.004299	-0.009530	0.004056	0.002838	-0.001564	0.000548
0.012229	0.008024	-0.004609	-0.001396	0.002895	-0.003295	-0.001562	-0.000113	-0.000362
-0.012077	0.009136	0.003254	-0.002831	-0.004192	0.010117	-0.000183	-0.004893	-0.001362
0.000104	-0.002382	-0.005083	-0.001823	0.008194	0.001727	-0.001223	-0.002544	0.002664
-0.003653	-0.000998	-0.002546	0.002437	-0.002591	0.002792	0.003591	0.000632	-0.004039
0.010684	0.000741	-0.009855	0.002205	-0.000010	-0.000711	-0.000757	0.000345	-0.000243
-0.005916	-0.005490	-0.002383	0.006657	0.005134	-0.004296	-0.003192	0.004913	0.002217
0.004353	-0.001923	-0.007939	0.003999	0.004739	-0.003451	-0.006443	0.002955	0.004493
D8	D9	D10	D11	D12	D13	D14	D15	D16
-0.011272	0.002846	-0.001170	-0.000407	0.000812	0.008404	-0.002065	-0.001662	0.000248
-0.011198	0.003294	-0.000476	-0.003636	0.000417	0.002301	-0.002516	0.003440	-0.000871
-0.011193	-0.001645	-0.003214	0.009410	0.005423	-0.000844	-0.004952	-0.002464	0.001424
-0.011835	0.001669	0.007104	-0.003379	0.001233	-0.000818	-0.002826	-0.001700	-0.001279
-0.006632	0.004342	-0.006716	0.002375	-0.003592	-0.003216	0.004734	0.001342	-0.001863
0.004306	-0.002327	0.001054	0.003229	0.001235	0.000249	0.000688	0.000810	-0.001537
0.014305	-0.004900	-0.004491	0.001323	0.007238	-0.001710	-0.002310	-0.000106	0.001007
-0.000790	-0.006040	-0.005224	0.004162	-0.000308	0.000077	-0.000052	-0.001035	-0.001808
0.000358	0.006046	0.008487	-0.003312	-0.004243	-0.000536	0.000058	-0.002739	0.000267

APPENDIX 4.

Scatterplots of scores from the Principal Component Analysis (PCA) on harmonic coefficients calculated for outlines of major hip bone foramina (source data in Appendix 3).



APPENDIX 5.

Left hip bone of an extant penguin *Eudyptula minor* (NHMUK/T 1881.1.17.105) showing the ilioischiadic membrane (lateral view). Abbreviations: at, antitrochanter; iif, ilioischiadic foramen; iim, ilioischiadic membrane; il, ilium; is, ischium; pb, pubis; pdp, correlate of proximal dorsal process; pfe, proximal femur (broken). Scale bar equals 1 cm.

